PERGAMON

Progress in Biophysics & Molecular Biology 74 (2000) 1–35

Progress in Biophysics & Molecular Biology

www.elsevier.com/locate/pbiomolbio

Review

Protein structural dynamics by single-molecule fluorescence polarization

Joseph N. Forkey*, Margot E. Quinlan, Yale E. Goldman

School of Medicine, University of Pennsylvania, Physiology Department, Pennsylvania Muscle Institute, D700 Richards Building, 3700 Hamilton Walk, Philadelphia, PA 19104-6083, USA

Contents

*Corresponding author.

PII: S0079-6107(00)00015-8

Keywords: Single molecule; Fluorescence; Polarization; Evanescent wave; Microscopy; Bifunctional; Dynamics; Total internal reflection

1. Introduction

The astonishing progress made during the last two decades toward understanding the machinery of cells has been fueled in large part by developments in structural biology, molecular biology, and biophysics. Thousands of protein structures have been solved at atomic resolution and the amino acid sequences and roles of many specific motifs are now known. While application of these techniques has greatly enhanced our understanding of the structure and biochemistry of proteins, elucidation of the quantitative relationships between structural changes in the proteins, enzymatic activity, signaling, energy conversion and macromolecular interactions will require further development of novel methods.

In this chapter we describe a new technique, single-molecule fluorescence polarization (SMFP), that has the potential to fill a void in conventional methods for determining the structural basis of protein activity. Using state-of-the-art optical microscopes and novel fluorescent probes attached to specific protein domains, SMFP makes it possible to quantify angular rotations that mediate function in individual protein molecules. To demonstrate the importance of protein domain rotational motions, this chapter begins with several examples of biophysical systems in which orientational changes are essential to their mechanism. This is followed by a discussion of the advantages of detecting such rotations with individual molecules and a brief synopsis of the development of SMFP and early experiments. The next two sections are devoted to technical considerations, including characteristics of extrinsic fluorescent probes, optical apparatus and data analysis. Finally, recent work using this technique is reviewed.

1.1. Protein rotational motions

Crystallographic studies of proteins trapped in several different configurations analogous to states of the functioning system often lead to hypotheses for the structural basis of the catalytic activity. They also identify likely sites of interaction with upstream and downstream functional partners. Distinct conformations are typically characterized by differences in the relative orientations of nearby compact domains linked by hinges or swivels composed of glycine residues or flexible loops. The implied rotations have direct bearing on the functional output as illustrated here by several examples where large orientation changes have been discovered.

Due to the helical structure of double-stranded DNA (dsDNA), nucleic acid processing enzymes produce a torque when unwinding the helix to gain access to the base sequence. These enzymes catalyze processes such as replication, transcription, repair and recombination.

Topoisomerase II removes accumulated strain in dsDNA and enables separation of chromosomes or untangling of circular DNA after replication. It operates by passing one dsDNA segment through a 'gate' temporarily created in another double-stranded segment. During passage of the intact dsDNA through the gate, quaternary structural changes in the DNA-opening platform take place. Dramatic reorganization of accessory protein domains include rotations of up to 170° (Fig. 1a; Fass et al., 1999).

During protein biosynthesis, two GTP-binding elongation factors (EF-Tu and EF-G) enable the ribosome to accurately translate the genetic code into amino acid sequences and to maintain the codon reading frame. In each elongation cycle of a nascent polypeptide, an aminoacylated transfer RNA (tRNA) binds to the ribosome as a ternary complex with EF-Tu and GTP. If the tRNA's anti-codon matches the codon in the template messenger RNA, EF-Tu hydrolyzes the GTP and dissociates. The amino acid is then transferred from the tRNA to the peptide. Crystal structures show a nearly 90° rotation between domains in EF-Tu accompanying GTP hydrolysis (Fig. 1b; Clark et al., 1999). The tRNA also rotates ~60° relative to the ribosome. EF-G participates in translocation of the mRNA and two tRNA molecules by exactly 3 bases along the synthetic machinery. Whether EF-G functions as a 'motor' and whether it exhibits large domain rotations are controversial (Rodnina et al., 1999).

The F_0–F_1 ATP synthase couples energy from a proton gradient across the inner mitochondrial membrane into phosphorylation of ADP to form ATP. This process is the major end product of mitochondrial respiration. F_0 is thought to be a motor that rotates a protein driveshaft (the γ subunit; Walker, 1994; Boyer, 1997). Torque transmitted to the F_1 domain drives the 'uphill' ATP synthetic reaction. When uncoupled from F_0, F_1 hydrolyzes ATP and rotates the γ subunit in the opposite direction (Yasuda et al., 1998).

Myosin, the motor protein in muscle contraction and in many types of non-muscle motility, translocates along the cytoskeletal filament, actin. In crystal structures of myosin with various nucleotide analogs bound, the angle between the region containing the actin and nucleotide binding sites (the motor domain) and that containing the myosin light chains varies by up to 70° (Fig. 1c; Rayment et al., 1993a,b; Dominguez et al., 1998; Houdusse et al., 1999; Corrie et al., 1999). These studies and other data suggest that during the enzymatic ATPase cycle, a tilting of the light chain domain amplifies sub-nanometer structural changes at the nucleotide binding site into several nanometers of motion (Goldman, 1998).

Voltage-gated ion channels underlie electrical impulses in the surface membranes of excitable cells such as neurons and muscle fibers. Na^+, K^+ and Ca^{2+} channels are all composed of homologous repeated domains that form a membrane-spanning pore. The channels are normally closed when transmembrane voltage is negative inside of the cell relative to the extracellular space, but they open when the potential decreases or reverses. The fourth membrane spanning segment (S4) within each domain contains positively charged residues and is thought to serve as the voltage sensor. X-ray crystallography of ion channels has been more difficult than for soluble proteins, but the structure of a homologous bacterial K^+ channel (without voltage gating) has recently been solved (Doyle et al., 1998). While this structure has resulted in many new insights, the motions associated with gating are still unknown. Experiments using fluorescent probes attached to S4 segments of eukaryotic K^+ channels, however, suggest that the voltage sensor either translates or tilts when the membrane electrical field is altered (Mannuzzu et al., 1996; Yang et al., 1996; Loots and Isacoff, 1998).

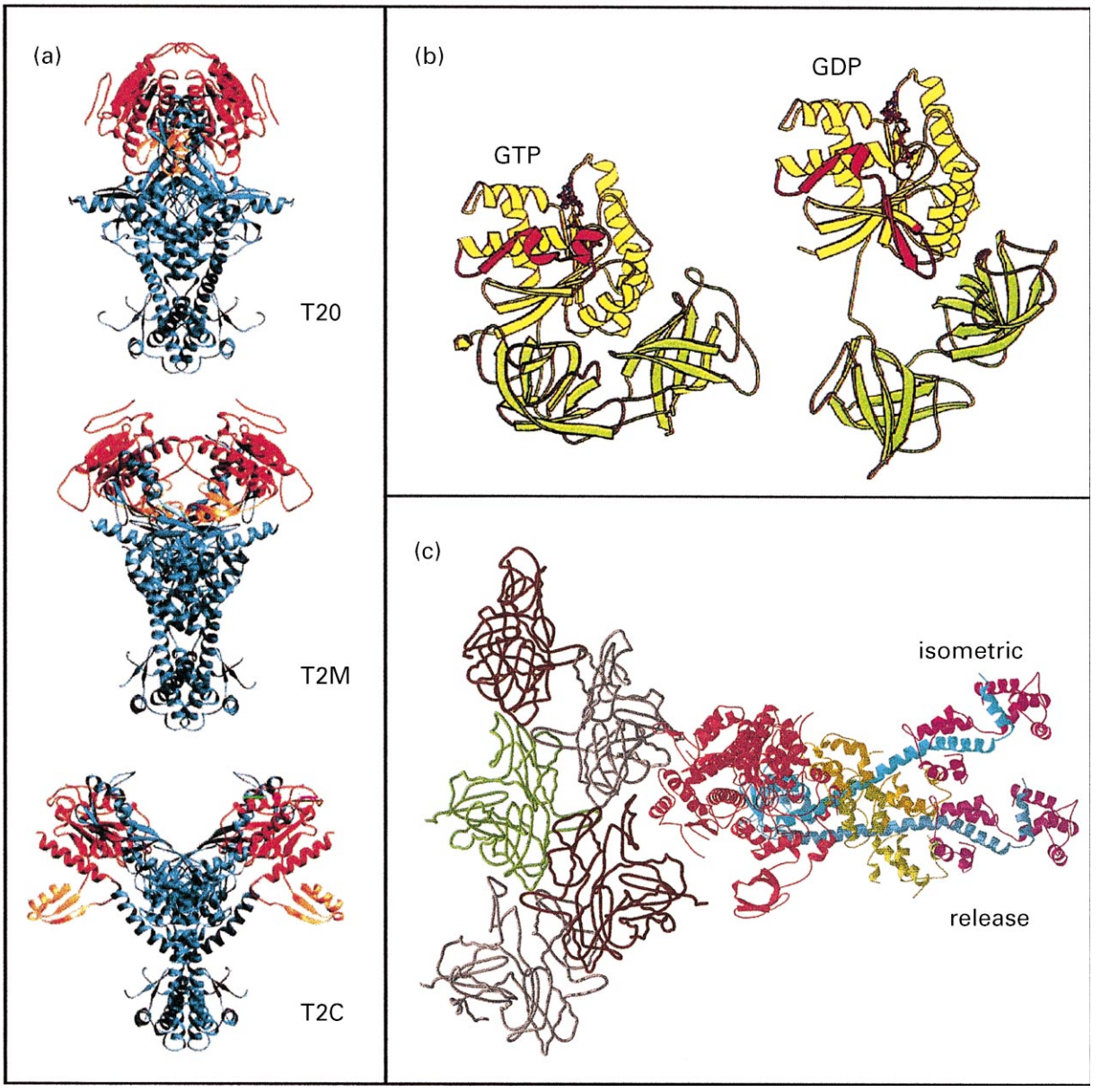

Fig. 1. Examples of crystal structures showing protein domain rotations. (a) Topoisomerase II (T2). Both the Rossman fold (red) and the B′ hook (orange) domains rotate relative to the DNA binding platform (blue) during activity. (Reprinted from with permission from Fass et al., 1999, Structural Biology, Nature 6, 322–326.) (b) Ribosomal elongation factor-Tu undergoes a large nucleotide-hydrolysis-dependent reorientation of domains. Note the relative positions of domain I (yellow) versus domains II and III (green) and the transition from α-helix to β-strand in Switch I (red). (Reprinted from FEBS Letters 452, Clark et al., "Structural information for explaining the molecular mechanism of protein biosynthesis" pp. 41–46 © 1999 with permission from Elsevier Science.) (c) Crystal structure of chicken skeletal muscle myosin subfragment-1 (red, blue, tan, and magenta) docked to actin (gray, brown and green; Rayment et al., 1993a). The angle of the light chain domain has been modified to show the relative orientation change determined from fluorescence polarization experiments with bifunctional rhodamine (see Section 2.1) when a muscle fiber is suddenly allowed to shorten during isometric contraction. (Reprinted from Corrie et al. "Dynamic measurement of myosin light-chain-domain tilt and twist in muscle contraction", Nature 400, 425–430 © 1999 with permission from Nature (http://www.nature.com/).

In all of these systems, plausible relationships have been proposed between the observed structural changes and the functional output. Many aspects, though, are unresolved. These include the kinetics of the events, the relationship to ATP or GTP hydrolysis and how each protein is controlled by the chemical, mechanical and topological states of its functional partners. Thus testing the structurally derived hypotheses requires detection of the timing and extent of the motions during activity.

1.2. Fluorescence polarization

While X-ray crystallography provides remarkable spatial resolution of long-lived, static states, it provides no temporal information on functionally relevant motions except in rare instances (e.g. Schlichting et al., 1990). Conclusions about the mechanism of activity must usually be inferred from the structures of a few trapped states. Furthermore, even these configurations are approximations of the native structures since the environment within a crystal is much different from the cytoplasm or membrane of a cell. In particular, the solvents and intermolecular forces within a crystal are usually unphysiological. Entire macromolecular complexes do not often crystallize, so the structural data are usually limited to subcomplexes, individual subunits or even products of proteolytic cleavage.

Nuclear magnetic resonance (NMR) also yields atomic spatial resolution and may be performed under aqueous conditions, often closer to a native environment. However, this technique is limited to small proteins ($<\sim$30–50 kDa) tumbling freely in solution (Pervushin et al., 1997; Wand et al., 1998). Electron spin resonance (EPR) provides unambiguous angular information and therefore, can also be used to detect domain rotations (Hubbell et al., 1996; Mchaourab et al., 1996). In samples containing multiple states of a reaction pathway, the kinetics of exchange between those states can often be determined by NMR or EPR (Cantor and Schimmel, 1980, Chapter 9). However, direct characterization of consecutive structural states on the time scale of an enzymatic pathway has been achieved with magnetic resonance techniques in only a few cases (e.g. Ostap et al., 1993; Hubbell et al., 1996; Mollaaghababa et al., 2000).

Spectroscopic techniques, including circular dichroism, birefringence, fluorescence resonance energy transfer, fluorescence quenching and Raman scattering, probe structural changes with ample time resolution to monitor functional changes (Cantor and Schimmel, 1980, Chapter 8). These methods often can be used with proteins in native conditions. The structural information provided, however, is usually ambiguous. Structural changes are inferred from a primary signal that is influenced by several parameters including distance between residues, relative orientation and local environmental conditions, such as hydrophobicity or solvent accessibility; sorting out the relative effects of these different factors is often difficult.

Fluorescence polarization provides a technique that bridges the gap between studies with atomic spatial resolution but poor time resolution and those with good time resolution but ambiguous structural information. This technique has been used extensively to detect structural changes in organized systems, such as proteins embedded in cell membranes or muscle fibers, or in isotropic suspensions of soluble proteins or vesicles (Lakowicz, 1999, Chapters 10, 11). In this review we apply the term 'bulk samples' to such experimental systems. Either intrinsic fluorescence is used or the target macromolecule is labeled specifically with an extrinsic fluorescent probe. By exciting the probe with polarized light and by resolving the polarization of

the fluorescence emission, the distribution of probe orientations and the time course and extent of probe motions can be determined. The measured polarization ratios are typically sensitive solely to probe orientation. However, a problem in relating this information to the orientation and dynamics of the protein motions in these studies has been that the probe orientations relative to the protein were not known. Newly synthesized probes, discussed in more detail below, which bind to the proteins at predetermined orientations, promise to eliminate this source of uncertainty.

1.3. Single-molecule fluorescence polarization

The single-molecule experiments discussed in this review represent extensions of the fluorescence polarization technique that has been applied to bulk samples. While measurements on macroscopic populations offer the advantage of producing large signals, there are several disadvantages. The average behavior of a population can be measured but some properties of the distribution are lost in the ensemble average. Inhomogenieties are not detected and apparent changes are diminished by asynchrony. By studying single molecules, these problems are avoided.

In bulk measurements, the information accessible about macromolecular orientation is limited by the sample geometry. Intensities of polarized fluorescence, and therefore the derived polarization and anisotropy ratios, depend on the orientational distribution of fluorophores. In suspensions, the rates and extent of probe motions can be interpreted in comparison to expected rates of tumbling, but the isotropic distribution furnishes no average orientation. The fluorescence anisotropy is sensitive to local probe orientation relative to the major hydrodynamic axes of the macromolecule and to internal flexibility of domains and secondary structural elements. In cylindrically symmetrical organized systems such as lipid bilayer membranes (Dale, 1988) and muscle fibers (Mendelson and Wilson, 1987; Hopkins et al., 1998), additional angular information is attainable because the molecules of interest are organized spatially around a symmetry axis. The angular distribution of probes can be measured relative to the axis of symmetry, but azimuthal angles around that axis are unavailable. In contrast, SMFP can completely determine a single fluorophore's mean orientation relative to a laboratory frame of reference which can then be transformed into any convenient coordinate system in the experimental sample.

Asynchrony of molecular transitions also hampers interpretation of bulk measurements. If the sample is undergoing a catalytic cycle, then every state of its reaction pathway will be populated to some extent and a measurement on the stationary system will reflect partitioning of the molecules among these states. In order to observe conformational changes between well-defined states, a perturbation can be imposed on the stationary distribution, such as a temperature or pressure jump, rapid addition of a substrate or photoliberation of a "caged" ligand (Gutfreund, 1995). These perturbations, however, provide a less than complete synchronization of the population, and furthermore, the synchronization degenerates over the same time scale as the processes of interest, due to the stochastic nature of the reactions. In SMFP, no synchronization is necessary. Any conformational state that persists longer than the time required to make a measurement (typically milliseconds) is potentially detectable from changes in the measured intensities. As described in Section 3, motions on time scales both faster and slower than the fluorescence lifetime can also be distinguished with SMFP.

Additional advantages of making fluorescence polarization measurements on individual molecules relate to uncommon or rare events. In the ensemble average from a bulk measurement,

signals from rare events are generally overwhelmed by signals from common processes. However, in a single-molecule experiment, rare events are observed directly. Similarly, kinetics in bulk experiments are usually sensitive to only a few 'rate limiting' steps, whereas single-molecule traces potentially reveal the lifetimes of all states persisting longer than the measurement time.

All of these advantages of SMFP follow from detection of the signal from an individual molecule rather than an average from a bulk population. A single molecule is a pure, homogeneous and synchronized sample. Analogous advantages apply to the other single-molecule techniques described in this volume.

1.4. Early single-molecule fluorescence experiments

A brief summary of major developments specifically relevant to SMFP measurements on biological samples is given here. The history of single-molecule detection, in general, has been reviewed extensively (Nie and Zare, 1997; Xie and Trautman, 1998; Moerner and Orrit, 1999; Weiss, 1999).

Some of the first successful efforts to detect individual molecules in solution by fluorescence spectroscopy involved labeling a single macromolecule with many ($\sim$100) fluorescent probes (Hirschfeld, 1976; Barak and Webb, 1981; Morikawa and Yanagida, 1981). The multiple dipoles precluded orientation analysis and extensive labeling tends to suppress biological activity. Detection of single fluorophores in aqueous solution was first demonstrated by Shera et al. (1990) using laser-induced fluorescence by illuminating a small volume of solution traveling through a flow cell and using time-gated detection to distinguish fluorescence from Raman scattering. Autocorrelation analysis produced convincing evidence that the signals were derived from individual molecules of rhodamine-6G.

Many early single-molecule experiments were conducted at very low temperatures and in solid substrates where reduction of thermal motion simplified detection and analysis. Under these conditions, single pentacene impurities in *p*-terphenyl crystals were detected using frequency modulated absorption spectroscopy (Moerner and Kador, 1989), and later by fluorescence spectroscopy (Orrit and Bernard, 1990; Ambrose and Moerner, 1991; Orrit et al., 1993). Measurements of the fluorescence intensity of similar crystals, while varying the excitation polarization, yielded discrete orientations of the individual pentacene dipoles projected onto the crystal plane (Güttler et al., 1993, 1996). This work resulted in assignment of the observed spectral properties to crystal lattice states.

Near-field scanning optical microscopy (NSOM) enabled investigation of single molecules at ambient temperatures (Betzig and Trautman, 1992; Betzig and Chichester, 1993; Ambrose et al., 1994; Trautman et al., 1994). In this technique, a sub-wavelength diameter light source is positioned very close to the specimen (Fig. 2a) on a microscope slide. The source is raster-scanned across the slide. By limiting the excitation volume, background fluorescence and scattering are kept much lower than the signal from a single molecule. Betzig and Chichester (1993) measured the orientation of carbocyanine dye molecules ($DiIC_{12}$) on polymethylmethacrylate (PMMA) coated slides. These experiments took advantage of the spatial distribution of optical polarization at the tip of the scanning probe to determine the three-dimensional orientation of single fluorophores, as shown in Fig. 2b. Using identical samples, Trautman and Macklin (1996) and Macklin et al. (1996) compared measurements made with NSOM and spot-confocal microscopy,

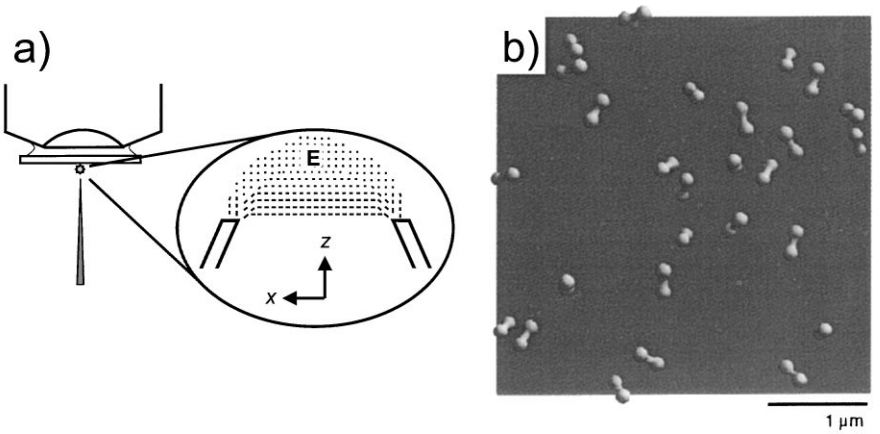

Fig. 2. (a) Near-field scanning optical microscopy utilizes a probe with diameter smaller than the wavelength of light. The probe is raster scanned across the sample. The electric field vector in the evanescent wave at the probe tip is indicated by the bars in the expanded view. (b) Dipole orientations of individual carbocyanine dye molecules determined from Near-field scanning optical fluorescence microscopy. (Reprinted with permission from Betzig and Chichester, ''Single molecules observed by near-field scanning optical microscopy'', Science 262, 1423–1424. Copyright (1993) The American Association for the Advancement of Science).

a far-field technique. These studies showed that NSOM provided better spatial resolution, as expected, as well as more complete orientation information. However, the much simpler far-field spot-confocal technique furnished more accurate measurements of excited state lifetime and higher temporal resolution. These experiments also demonstrated the orientation sensitivity of the far-field technique by exciting with two orthogonal polarizations. Using analysis procedures described below, the two resulting fluorescence intensities were combined to determine the orientation of the absorption dipole projected onto the plane of the microscope stage.

Refinements to epifluorescence microscopes using laser excitation sources enabled two groups to detect single labeled proteins under aqueous conditions appropriate for functional activity (Funatsu et al., 1995; Sase et al., 1995). Funatsu et al. (1995) also used the evanescent wave generated by total internal reflection as an excitation source and obtained an additional reduction of background compared to laser epifluorescence. They showed that kinetics of single enzymes can be studied by measuring interaction of a fluorescent ATP analog with individual fluorescently labeled myosin molecules. Sase et al. (1995) recorded continuous images of actin filaments, sparsely labeled with tetramethylrhodamine, as they were propelled by myosin in an in vitro motility assay. These pioneering studies inspired many of the SMFP experiments summarized later in this review by establishing that single functioning protein molecules could be monitored in real time.

2. Experimental methods

This section presents an overview of methods used for SMFP experiments. Many suitable fluorescent probes are available for labeling the protein (or macromolecular system) under investigation, the choice being dictated by optical and biological considerations. A variety of

optical arrangements with low background and high sensitivity have been developed to detect individual probes. The excitation methods generally minimize background signal levels by illuminating a very small volume. The detectors possess high sensitivity and low intrinsic noise. The discussion here is limited to details of particular relevance to SMFP. More general descriptions of methods for single-molecule microscopy may be found in several recent reviews (Basché et al., 1997; Nie and Zare, 1997; Xie and Trautman, 1998) and other chapters in this volume.

2.1. Fluorescent probes

The use of intrinsic fluorescence and the available extrinsic fluorescent probes have been reviewed (Haugland, 1996, Chapter 1; Johnson, 1998; Lakowicz, 1999, Chapter 3). Rhodamines, Cy3, Cy5, Green Fluorescent Protein (GFP), Texas Red, pentacene and $DiIC_{12}$ have all been used in single-molecule investigations and others may be applicable. High quantum yield for fluorescence emission (Q_f) and photostability are especially desirable characteristics for SMFP due to the low signal levels. The total number of photons emitted by an individual molecule before it is irreversibly photobleached must be high enough to obtain sufficient signal levels over a useful time period (typically 0.1–10 s for protein studies). Total photon emission is approximately equal to the ratio of Q_f to the quantum yield for photobleaching (Q_b). Rhodamine and Cy3 are examples of probes with high Q_f/Q_b ratios. When photobleaching is minimized by eliminating reactive oxygen in the medium, $\sim 10^6$ fluorescent photons are emitted by these probes before irreversible photodestruction (Soper et al., 1991; Nie and Zare, 1997).

In fluorescence polarization studies, close alignment of the probe's absorption and emission transition dipole moments is advantageous since it simplifies data analysis. This characteristic is quantified by r_o, the fluorescence anisotropy of a sample containing randomly oriented immobilized probes or the zero-time anisotropy in nanosecond time-resolved measurements of freely rotating probes. r_o equals 0.4 for probes with perfectly aligned absorption and emission dipoles. For instance, for the major visible absorption transition in rhodamine and other xanthene derivative fluorophores (e.g. fluorescein, eosin, etc.), $r_o \cong 0.38$ (Chen and Bowman, 1965; VanderMeulen et al., 1990; van der Heide et al., 1992) indicating that the two dipoles are aligned to within $\sim 10^\circ$. In this case, the reasonable assumption is commonly made that the absorption and emission dipoles are colinear.

In experiments using extrinsic probes, the extent and specificity of labeling should be considered and functional characteristics of the labeled protein should be compared to those in the native state. Probes are available with reactive linkers that target specific residues which can be engineered into the polypeptide sequence to place probes at particular locations. Many examples of site-specific labeling of surface residues at high stoichiometry and with relatively little perturbation of activity have been reported (Maxfield, 1989; Wang, 1989; Waggoner, 1995; Mchaourab et al., 1996; Sabido-David et al., 1998).

Green fluorescent protein (GFP) and its derivatives (Cubitt et al., 1995; Heim and Tsien, 1996; Tsien, 1998; Yang et al., 1998) have been used widely in cell biological studies because they can be easily linked to many proteins and introduced into the native environment. GFP is well polarized ($r_o = 0.32$; Swaminathan et al., 1997). However, GFP has not been effectively utilized in SMFP studies because its emission is not stable. It exhibits transient periods of zero fluorescence — a phenomenon that has been termed 'blinking' (Dickson et al., 1997; Pierce et al., 1997). Instability

of emission causes intensity changes unrelated to probe orientation and, therefore, fluorescence polarization data from GFP are difficult to analyze. Blinking has also been observed with other fluorophores (e.g. Ha et al., 1996).

The fluorophore orientation that gives rise to experimental fluorescence polarization signals reflects both the protein orientation and the angular position of the probe relative to the protein. Typically, the latter angle is not known and may even be inhomogeneous. Given these uncertainties, it is generally not possible to determine the orientation of a protein domain from the measured orientation of the probe dipoles, a major limitation of fluorescence polarization studies. Recent developments, however, circumvent this difficulty by fixing the probe to two or more amino acids, thereby defining the local orientation.

A bifunctional rhodamine (BR) (Fig. 3a and b) was synthesized by Corrie et al. (1998) to bind to two appropriately spaced cysteine residues engineered into a protein. The absorption and

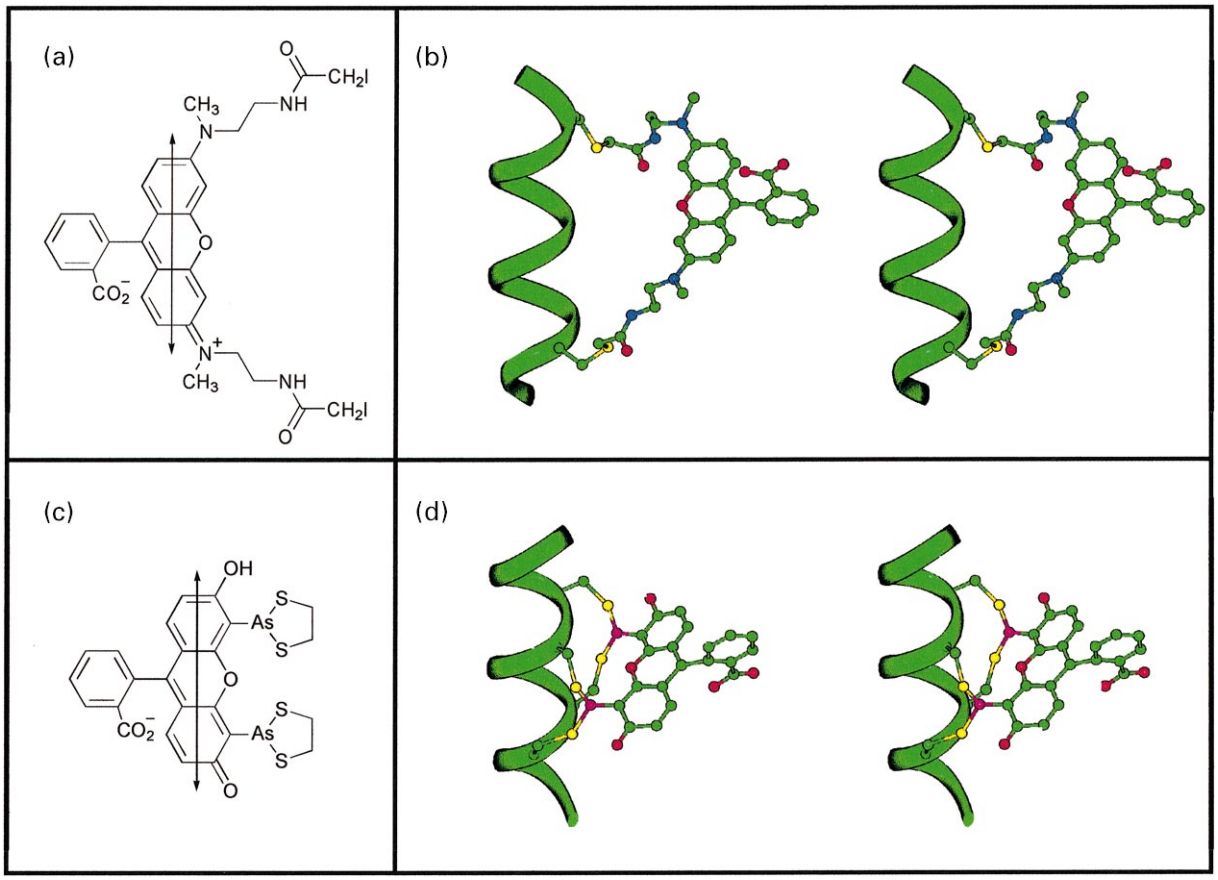

Fig. 3. New probes which can be bound with known location and orientation to an engineered protein. (a) Bisiodoacetamidorhodamine (BR-I_2), (b) stereo view of bifunctional rhodamine (BR) crosslinked to two cysteines in an α-helix, (c) 4′,5′-bis(1,3,2-dithioarsolan-2-yl)fluorescein (FlAsH-EDT_2), (d) stereo view of FlAsH bound to four cysteines in an α-helix. The FlAsH chromophore is depicted in one of two possible orientations (see text). The absorption and emission transition dipole moments are shown as double-headed arrows in (a) and (c).

emission dipoles in rhodamine are aligned with the long axis of the aromatic ring system that forms the chromophore (double-headed arrow in Fig. 3a). The two iodoacetamide linkers on the ends of the chromophore can bind covalently to accessible cysteine residues suitably spaced in the protein. The orientation of the dipoles relative to the protein is then expected to be along a line between the two cysteine residues which is known from the atomic structure. In order to detect rotations about different protein axes, various relative orientations can be obtained by replacing different pairs of native amino acids with cysteines.

Bifunctional rhodamine has been applied to the study of the myosin regulatory light chain (RLC) orientation in muscle fibers (Corrie et al., 1999). Four mutants were constructed, each containing a pair of cysteine residues 1.0–1.6 nm apart. These mutant proteins were reacted with the bifunctional rhodamine and the 1 : 1, two-site labeled protein was isolated from the reaction mixture by FPLC. The probe was shown to bind specifically and cross-link the pair of engineered cysteine residues in each mutant. In combination, the data from the four mutants enabled determination of the motions of the RLC relative to the muscle fiber axis in steady-state experiments and in dynamic measurements with 50 μs time resolution. BR may find many applications in single-molecule studies of myosin and other systems.

Another probe designed to provide a stable, uniform orientation relative to the protein is 4′, 5′-bis(1,3,2-dithioarsolan-2-yl)fluorescein (FlAsH-EDT_2; Fig. 3c; Griffin et al., 1998). FlAsH is an organoarsenical compound that binds tightly to a protein α-helix containing cysteines at positions i, $i+1$, $i+4$ and $i+5$ (Fig. 3d). Native residues are replaced by cysteines to position this amino acid motif at a known orientation with respect to the crystal structure. Whether the chromophore is oriented along the $i \leftrightarrow i+4$ direction or $i \leftrightarrow i+1$ (or both) is not currently known, but its rotational mobility is restricted when it interacts with calmodulin containing the binding motif (S.R. Adams, pers. comm.). The FlAsH reagent itself is virtually non-fluorescent but becomes fluorescent upon binding to the four cysteine residues of the target protein. Thus, appearance of fluorescence is an indicator of specific labeling. Excess ethanedithiol (EDT) can reverse this reaction, and dissociate FlAsH from the protein. These features enable FlAsH to be used both in vitro and inside live cells.

The two fluorescent probes with multiple linkers mentioned here have been synthesized in academic laboratories. Other bifunctional fluorescent compounds have recently become available commercially (Ehrhardt et al., 1998). As the value of this new type of probe becomes more evident, other bifunctional or motif-specific labels should become available.

2.2. Instrumentation

In most SMFP experiments the sample under study is immobilized on a surface or in a polymer matrix (Dickson et al., 1996; Lu et al., 1998) to constrain individual molecules within the field of view long enough for their reaction processes to be observed. Either the sample sparsely occupies the detected volume or it is sparsely labeled with probes so that individual fluorophores are spatially separated and distinguishable. The surface interaction may also provide a fixed orientation of the attached domain. Rotational motions are then referred to that stable platform. Samples can be attached to glass (Howard et al., 1993, Unger et al., 1999), fused silica (Iler, 1979, Chapters 6, 7; Funatsu et al., 1995; Sase et al., 1995) or freshly cleaved mica surfaces (Bopp et al., 1997; Sytnik et al., 1999). Methods for attaching motor and cytoskeletal proteins to surfaces have

been discussed by Scholey (1993). Nitrocellulose, a surface coating commonly used to attach myosin to glass coverslips, exhibits fluorescence, presumably due to contaminants (Conibear et al., 1998), that limits its usefulness in SMFP. Other methods for sample attachment to surfaces are described in the studies cited below and in other chapters in this volume.

The sample slide is placed on the stage of an upright or inverted microscope fitted with polarizing optics and a sensitive detector. The input optics are arranged to limit the excitation electric field to a very small volume (Nie and Zare, 1997). This minimizes background fluorescence from contaminants and from labeled proteins elsewhere in the sample chamber. It also reduces the amount of Rayleigh and Raman scattering from the buffer itself. A high numerical aperture (NA) microscope objective is used to collect as large a fraction of the emitted fluorescence as possible and to project the emission through bandpass or long-pass spectral filters and polarizing optics to the detector.

Lasers are ideal excitation sources for SMFP measurements because of their spectral purity, coherence, and high degree of polarization. Emission from a standard polarized laboratory laser generally exhibits a high extinction ratio (typically on the order of 100 : 1). A 'clean-up' polarizer can improve the linear polarization to achieve an extinction ratio of 10^4 : 1 or better (for a technical discussion, see e.g. catalogs of Melles Griot Corp., 1999, Chapter 1, or Newport Corp., 1999, Chapters 8, 11). Comparing emission intensities for different excitation polarizations enables determination of the orientation of the probe absorption dipole as explained below in Section 3. The polarization angle can be altered by mechanically switching linear polarizers or by rotating a retardation plate. Faster modulation of the polarization (in the μs range) is achieved using electronic variable retarders (Jenkins and White, 1976, Chapter 32).

Power of the excitation light influences the intensity of fluorescence, as well as the photobleaching rate. An increase in excitation power will increase the emitted photon flux proportionally, and therefore, increase the signal-to-noise ratio (Inoué and Spring, 1997, Chapter 6). However, because the number of photons emitted by a fluorophore before photobleaching is limited, such an increase in excitation power will also accelerate photobleaching. Therefore, a tradeoff exists between signal-to-noise ratio for individual measurements and total recording time before photobleaching. Also, the excitation power should be kept low enough so that the absorption probability is linear in intensity (i.e. the fluorophore should not be saturated; Yariv, 1975, Chapter 8). The absolute intensity is difficult to quantify, so orientation measurements are usually made by comparing two or more emission intensities with different excitation and/or detection polarizations (Lakowicz, 1999, Chapter 10). Reliable determination of calibration factors that quantify the relative excitation power and detection sensitivity at different polarizations is crucial for this type of experiment. Measurements on a sample with known polarization properties are used to determine these factors. This is similar to the determination of the instrument factors in a conventional spectrofluorimeter.

2.2.1. Far-field excitation

With relatively minor modifications, a standard research epifluorescence microscope may be used to perform SMFP experiments (Funatsu et al., 1995; Sase et al., 1995; Unger et al., 1999). Usually, a laser excitation source replaces the arc lamp illuminator. The objective and immersion fluid are selected for low autofluorescence. The laser is either focussed or collimated at the back focal plane of the objective, leading to wide-field epiillumination or spot-confocal excitation

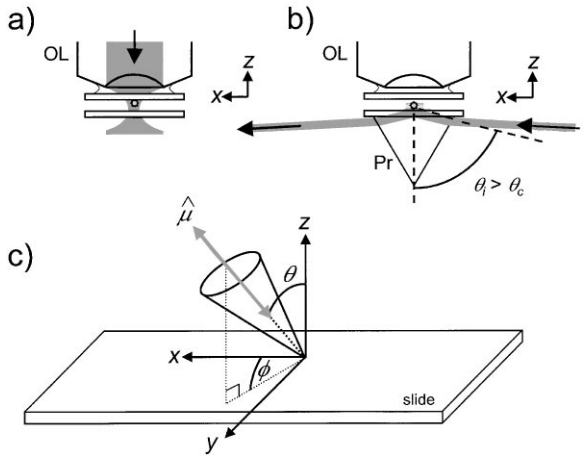

Fig. 4. Fluorescence excitation schemes. (a) With laser spot-confocal excitation, a laser beam is focused through the objective lens (OL) to a diffraction limited spot. (b) Prism (Pr)-type total internal reflection produces an evanescent wave near the microscope slide/buffer interface. (c) Cartesian coordinate system used in Section 3 and Appendix A. The origin is on the microscope slide. The x- and y-axis are in the plane of the slide. The z-axis coincides with the optical axis of the microscope and points towards the objective. The orientation of a transition dipole moment, $\hat{\mu}$, is described by its polar angles θ (axial) and ϕ (azimuthal).

(Fig. 4a) at the slide surface, respectively. Diffraction limited illumination and detection of emission from the same small volume in laser spot-confocal microscopy provides high spatial resolution and minimizes fluorescence from other regions of the sample (Pawley, 1995). The sample is scanned in order to obtain a two-dimensional image of the slide surface. Wide-field epiillumination avoids the necessity for lateral scanning of the excitation at the expense of higher background.

For either of these far-field excitation techniques, using a Gaussian mode laser, the excitation beam at the slide surface propagates predominantly along the optical axis (z-axis) of the microscope. The optical polarization (direction of the oscillating electric field) is thus predominately in the plane of the slide (x- and y-axis; Fig. 4c; see Xie and Trautman, 1998, for an exception). As will be discussed in more detail in Section 3, this characteristic of far-field propagating excitation makes it difficult to use for measuring the axial polar angle, θ, of the molecular orientation with respect to the z-axis.

2.2.2. Total internal reflection excitation

Total internal reflection (TIR) microscopy (Fig. 4b) makes use of the evanescent wave formed beyond a reflecting surface under glancing illumination. The input laser beam is directed through a glass or fused silica microscope slide toward the interface with the aqueous medium containing the experimental sample (see Axelrod (1989a) and Ambrose et al. (1999) for other possible geometries). The index of refraction (n_1) of the slide is greater than that of the medium (n_2). If the incident angle (θ_i with respect to the slide normal) is greater than the critical angle defined by $\theta_c = \sin^{-1}(n_2/n_1)$, then all of the energy is reflected back into the slide. The electric field, however, does not vanish abruptly at the surface. An oscillating electromagnetic field, termed an evanescent wave, is present on the aqueous side of the interface (Axelrod, 1989a). The evanescent wave is

capable of exciting fluorophores (Carniglia et al., 1972). Its amplitude decays exponentially away from the interface and, under conditions applicable to TIR microscopy, the $1/e$ decay constant is only a few hundred nm ensuring that only fluorophores at or near the surface are excited. Thus, contaminants and sample molecules in the bulk medium are not excited, reducing background several orders of magnitude as compared to conventional epifluorescence microscopy (Funatsu et al., 1995).

The evanescent wave has unusual but predictable polarization properties. Consider the geometry in which the scattering plane, which is defined by the incident and reflected beams, is the x–z plane (see Fig. 4b). If the incident beam is polarized perpendicular to the scattering plane (s-polarization), then the evanescent wave is polarized in the y direction (see Fig. 4c). If the incident beam is polarized parallel to the scattering plane (p-polarization) then the evanescent wave is polarized predominantly along the z direction, with a small component along the x direction (Axelrod et al., 1984). The relative magnitudes of the z- and x-component of polarization depend on n_1/n_2 and θ_i. For a typical setup with p-polarized excitation, the ratio of intensities (x-component/z-component) is approximately 0.05. As discussed further in Section 3.3, the robust z-component of polarization in the evanescent wave allows sensitive detection of the fluorophore orientation (θ) relative to the optical axis.

2.2.3. Near-field optical probe excitation

Near-field scanning optical microscopy is the optical equivalent of atomic force microscopy. A tapered optical fiber, coated with metal, serves as a near-field optical probe. Even though the probe aperture is smaller than the wavelength of the excitation light, a non-propagating oscillating electric field extends several hundred nanometers beyond the tip (Fig. 2a). As in TIR microscopy, this evanescent wave has predictable spatial extent and polarization. The shape of the electric field distribution provides various polarizations, including z-axis components, as the probe is scanned near an individual fluorophore (Fig. 2a; Dürig et al., 1986; Betzig and Chichester, 1993). The orientation of the electric field can also be altered by changing the polarization of the input light (Xie and Dunn, 1994; Ruiter et al., 1997).

A unique advantage of NSOM is that spectroscopic and topographic information can be measured simultaneously. Disadvantages are low-power throughput, poor reproducibility of the field distribution at the tip and the possibility of mechanical or electromagnetic perturbation of the sample by the probe (Macklin et al., 1996; Trautman and Macklin, 1996). Time resolution depends on the scanning area and signal-to-noise ratio, but is typically lower than with the spot-confocal, wide-field epiillumination or TIR methods.

2.2.4. Microscope objectives and emission optics

Because the signal-to-noise ratio in SMFP is limited by the number of detected photons, collection efficiency of the microscope objective is often more important than spatial resolution, flatness of field or correction of optical aberrations. Thus the numerical aperture and transmittance of the objective are the key specifications. When the excitation laser passes through the objective, a further requirement is very low autofluorescence.

The large solid angle subtended by high NA objectives complicates the data analysis somewhat due to the following effect. An individual fluorophore emits over a wide angle. When this light is collected and collimated by the objective, it is redirected to propagate along the optical axis (i.e.

the z-axis). Because the electric field remains normal to the direction of propagation for each ray, the polarization is also redirected by the objective. The effect of this refraction in regards to SMFP is that polarization originally along one axis of the microscope coordinate system is transferred partly onto the other two axes (Axelrod, 1989b). This depolarization must be taken into account as explained in Section 3.

The light collected by the objective lens is filtered in order to reject wavelengths outside of the fluorescence emission band. Stray light from the excitation beam as well as Raman and Rayleigh scattering are the greatest sources of background contamination (Nie and Zare, 1997). High-quality optical long-pass and band-pass filters are commercially available. The excitation wavelength may be further suppressed with sharp holographic notch filters which have recently become available.

Dichroic beamsplitters, filters, or mirrors are often used to redirect the emitted light. Care must be taken to account for polarization-dependent transmissions, reflections, and phase shifts (Born and Wolf, 1964, Section 1.5; see also Newport Corp. catalog, 1999, p. 11.14). This is particularly important if the light is not collimated, or when the detected polarization is not parallel or perpendicular to the reflection plane defined by the propagation direction of the incident light and the normal to the mirror. In these cases mixing between the detected polarization signals is possible. Similar precautions apply when reflecting surfaces are used in the excitation pathway.

Either total fluorescence is detected or orthogonal components of polarization are selected by a polarizer (analyzer). Hereafter, the term detector polarization will be used to denote the polarization transmitted by the analyzer. Simultaneous detection of both x- and y-polarization by using a polarizing beam splitting prism (e.g. a Wollaston or Thompson prism) and directing the polarized components onto two separate detectors is a common arrangement (Fig. 5a) because this scheme utilizes all of the collected light. A variant of this arrangement is the 'dual-view microscope' (Kinosita et al., 1991; Sase et al., 1997). The two polarization components are projected onto two-halves of the detector surface in a single video camera to simultaneously obtain spatial resolution and polarized fluorescence (Fig. 5b).

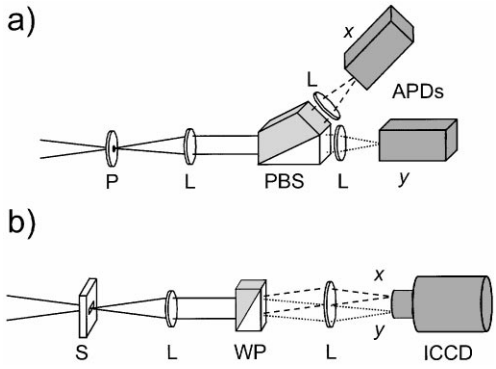

Fig. 5. Fluorescence detection schemes. (a) Emitted fluorescence is resolved into its two orthogonal components (here, x and y) with a polarizing beam splitter (PBS) and focused onto two separate avalanche photodiodes (APDs). (b) Emitted fluorescence is split by a Wollaston prism (WP), and imaged onto two halves of the detector area of an ICCD camera (Kinosita et al., 1991). L, lens; P, pinhole; S, slit.

2.2.5. Detectors

The light collected from individual fluorophores in SMFP experiments is ~10,000 photons per second or less, thus necessitating highly sensitive detectors. For single-molecule experiments in which localization of the molecule is the primary goal, a signal-to-noise ratio of 2 may be sufficient. However, for SMFP experiments, the accuracy of the deduced orientations is directly related to the measurement precision of the various polarized intensities and thus to the signal-to-noise ratio. The specific characteristics of a detector that govern the signal-to-noise ratio include the quantum efficiency, intrinsic background noise, and the fidelity of the amplification and readout processes. The time resolution of the detector is also important in dynamic experiments. Either solid-state (CCD) cameras or avalanche photodiodes have been used in most SMFP experiments.

Cameras offer the obvious advantage of simultaneously collecting data from a two-dimensional field on the microscope slide (Inoué and Spring, 1997, Chapters 7, 8). Slow scan, digital readout, back illuminated CCD cameras are available with very high quantum efficiencies (as high as 90% at 600 nm) and low combined readout and background noise (e.g. less than 10 counts per pixel per image). However, these cameras usually require several seconds to transfer data from an entire image. While data acquisition rates can be increased by binning pixels, or using on-chip frame transfer technology, slow-scan cameras are generally not fast enough to observe biologically relevant events in real time. CCD cameras coupled to image intensifiers offer considerably higher readout rates with transfer times for an entire frame as short as 30 ms and even faster subframe transfer times. The tradeoff for improved time resolution is a lower quantum efficiency (typically peaking at 40% near 550 nm) and higher measurement uncertainty caused by the statistical nature of the intensifier gain.

In SMFP, measurements of polarized fluorescence from individual stationary molecules have been made almost exclusively with avalanche photodiode (APD) detectors. These photon counting devices have an active area a few hundred μm in diameter, peak photon detection efficiency (including quantum efficiency) of ~70% at 700 nm, dark noise as low as 25 counts per second and maximum counting rates up to 10 MHz (Dautet et al., 1993) and manufacturer data sheets cited there. Thus, they impose no restriction on the measurement time resolution, which is then limited only by photon statistics.

3. Analysis of single-molecule fluorescence polarization data

Single-molecule fluorescence polarization data consist of a number of intensity measurements made with different excitation and detector polarizations. To analyze these data, the dependence of the intensities on molecular orientation and motions must be considered. Relationships of polarized fluorescence intensities to fluorophore orientation and mobility appropriate for SMFP data are presented here, in the appendix, and the references therein. The equations assume that a fluorescent molecule with non-degenerate, linear, absorption and emission transition dipole moments is excited by an electromagnetic field with known polarization, and that fluorescence is collected by a high NA objective lens. The excitation is assumed to be non-saturating so that the signal is linearly proportional to excitation intensity. The equations assume that the data have been corrected for background light and for

polarization-dependent variations in excitation intensity and detector sensitivity (instrumental artifacts).

The analysis given here does not account for Fresnel reflections at optical interfaces or for non-propagating components of dipole emission. These effects introduce only small perturbations for molecules more than a few wavelengths from the cover slip on the objective side of the sample chamber. However, the corrections may be larger for molecules on the surface of the cover slip if an oil immersion objective is used. In this case, non-propagating emission toward the objective may be converted into propagating radiation in the cover slip and contribute to the measured intensity. These effects, which are discussed by Hellen and Axelrod (1987), may change the quantitative analysis, but do not alter the types of information that can be obtained.

For the purposes of this discussion, it will be useful to define a number of distinct time scales of possible molecular motion. These are defined relative to the fluorophore's excited state lifetime, typically 1–10 ns, and relative to the time required for a single intensity measurement, typically 1–10 ms for photon counting experiments, or 33 ms for video imaging. Changes in molecular orientation that occur on a time scale much longer than the measurement time will lead to changes in measured intensity between successive data samples. Functionally related conformational changes may cause this behavior. A molecule undergoing such motion may be considered static for analyzing each individual measurement. The analysis for this case is the most straightforward, and will be considered first.

Following that, molecular motion with a time scale shorter than the measurement time will be considered. While a single equation may, in principle, account for any motion of this type, two limiting cases are of particular interest. "Fast wobble" will refer to the case of motion with a time scale much shorter than the fluorescence lifetime. Independent thermal vibrations of the probe may occur in this time regime. "Slow wobble" will refer to motions with a time scale much longer than the fluorescence lifetime, but still much shorter than the measurement time. Such rotations are likely to result from thermal motions of protein domains or from steps in the enzymatic reaction pathway. Motions in these characteristic time regimes confer distinct characteristics on the measured intensities. Furthermore, these cases are useful because often a small fluorescent probe will undergo fast wobble relative to its attachment point on a protein, while the protein (and attached probe) may exhibit slow wobble relative to the laboratory frame. While not treated explicitly here, the equations for slow wobble and for fast wobble may be combined to take into account motions on both time scales.

3.1. Stationary fluorophores

If the fluorophore is effectively stationary during the measurement time, the analysis provides the polar angles, θ and ϕ, of the absorption and/or emission dipole, as defined by the coordinate system shown in Fig. 4c.

3.1.1. Absorption polarization ratios

Switching between two excitation polarizations parallel to the x- and y-axis, and collecting the emitted fluorescence with a high NA objective lens, results in two measured intensities. As shown

in the appendix, these measured intensities are proportional to the projections of the absorption transition dipole moment onto the directions of polarization (i.e. along the x- and y-axis):

$$\begin{aligned} {}_{x}I &\propto \sin^2\theta_a \cos^2\phi_a \\ {}_{y}I &\propto \sin^2\theta_a \sin^2\phi_a \end{aligned} \tag{1}$$

where θ_a and ϕ_a are the polar angles of the absorption dipole, and the subscripts preceding I indicate the polarizations of the excitation light. In order to eliminate unknown multiplicative factors which are common to both measured intensities, including laser power, absorption cross section, objective collection efficiency, etc., an absorption polarization ratio, Q, may be calculated:

$$Q \equiv \frac{{}_{y}I - {}_{x}I}{{}_{y}I + {}_{x}I} = \frac{\sin^2\theta_a\left(\sin^2\phi_a - \cos^2\phi_a\right)}{\sin^2\theta_a\left(\sin^2\phi_a + \cos^2\phi_a\right)} = 1 - 2\cos^2\phi_a. \tag{2}$$

ϕ_a may then be determined from Q, which ranges from –1 to +1 as ϕ_a ranges from 0 to $\pi/2$. Note that due to the mirror symmetry of the transition dipole, optical techniques cannot differentiate between probe orientations (θ_a, ϕ_a) and $(\pi - \theta_a, \pi + \phi_a)$. For measurements using only linear polarizations along the x-, y- and z-axis, a further four-fold ambiguity arises in the determination of orientation due to reflection symmetries.

In order to increase accuracy, and to partially resolve this symmetry problem, measurements may be made at additional excitation polarizations. For an excitation laser with polarization in the plane of the stage and at an angle ζ with respect to the x-axis, the fluorescence intensity is given by (see Appendix A)

$${}_{\zeta}I \propto \sin^2\theta_a(\cos\phi_a\cos\zeta + \sin\phi_a\sin\zeta)^2 = \sin^2\theta_a\cos^2(\zeta - \phi_a). \tag{3}$$

As ζ is varied continuously, the phase of the intensity change gives ϕ_a.

3.1.2. Emission polarization ratios

The orientation of the emission dipole of a static molecule may be interrogated by resolving the polarization of the fluorescence. In analogy to the excitation case, the intensity of the emitted light detected through the analyzer is dependent mainly on the projection of the emission dipole onto the detector polarization axis. However, due to collimation of the light collected over the large solid angle subtended by a high NA objective, the detected intensity will also have some smaller contributions from components of the emission dipole perpendicular to the detector polarization. The extent of mixing of contributions from orthogonal components of the emission dipole depends on the numerical aperture of the objective as described in Appendix A. The intensities of detected fluorescence with polarizations along the x- and y-axis are given by

$$\begin{aligned} I_x &\propto C_1\sin^2\theta_e\cos^2\phi_e + C_2\sin^2\theta_e\sin^2\phi_e + C_3\cos^2\theta_e, \\ I_y &\propto C_2\sin^2\theta_e\cos^2\phi_e + C_1\sin^2\theta_e\sin^2\phi_e + C_3\cos^2\theta_e, \end{aligned} \tag{4}$$

where the subscript after each I indicates the polarization component detected, and θ_e and ϕ_e are the polar angles of the emission dipole. The coefficients C_1, C_2 and C_3 take into account the effects of the numerical aperture (see Appendix A and Axelrod, 1989b). For a water immersion objective with a typical numerical aperture of 1.2, $C_1 = 0.76$, $C_2 = 0.01$, and $C_3 = 0.23$. Calculating the

emission polarization ratio, P, from the intensities in Eq. (4) yields

$$P \equiv \frac{I_y - I_x}{I_y + I_x} = \frac{(C_1 - C_2)\left(\sin^2\phi_e - \cos^2\phi_e\right)\sin^2\theta_e}{(C_1 + C_2)\sin^2\theta_e + 2C_3\cos^2\theta_e}.$$
$$= \frac{(C_1 - C_2)\left(\sin^2\phi_e - \cos^2\phi_e\right)}{(C_1 + C_2) + 2C_3\cot^2\theta_e}. \quad (5)$$

P is sensitive not only to ϕ_e, but also to θ_e due to the high numerical aperture of the objective. The extent of the ratio's dependence on θ_e may be considered by comparing the relative magnitudes of $2C_3$ and $(C_1 + C_2)$. For the objective mentioned above, $2C_3 = 0.46$, while $(C_1 + C_2) = 0.77$. In principle, this polarization ratio may be combined with another measurement to determine both polar angles. For example, if the absorption and emission dipoles are colinear with polar angles $(\theta_a, \phi_a) = (\theta_e, \phi_e) \equiv (\theta, \phi)$, then the absorption polarization ratio in Eq. (2) will give the azimuthal angle, ϕ, and the emission polarization ratio can then be solved for the axial angle, θ.

Note that for fluorescence from a single stationary molecule, absorption polarization ratios are independent of the detector polarization, as indicated by Eq. (2). Emission polarization ratios (e.g. Eq. (5)) are independent of the excitation polarization. This is in striking contrast to the analogous measurements on bulk samples where, even if the molecules are stationary, the absorption polarization ratio depends on the detector polarization and the emission polarization ratio depends on the excitation polarization. For example, the excitation source preferentially excites a subpopulation of molecules aligned along its polarization. This photoselection biases the polarization of the emitted light.

For a stationary single molecule the measured fluorescence *intensities* (corrected for instrumental artifacts) depend on both excitation and detection polarization; however, the *ratios* do not. Regardless of how the molecule is excited, polarization of the emitted light is determined solely by the orientation of the emission dipole. Analogously, the probability of excitation depends only on the angle between the excitation polarization and the molecular absorption dipole. Thus, absorption polarization ratios do not depend on the detector polarization.

3.2. Non-stationary molecules

The general form of the equation describing polarized fluorescence intensity from a molecule undergoing rotation during an individual measurement is

$${}_{\varepsilon}I_{\alpha} = K\int_0^{\infty}\iiint \rho(\theta_a, \phi_a, \theta_e, \phi_e, t)(1/\tau)e^{-(t/\tau)}P_a(\theta_a, \phi_a, \hat{\varepsilon})P_e(\theta_e, \phi_e, \hat{\alpha})\,d\Omega_a\,d\Omega_e\,dt \quad (6)$$

(see also Cantor and Schimmel, 1980, Section 8-2). Here, $\rho(\theta_a, \phi_a, \theta_e, \phi_e, t)$ is a correlation function which describes the probability density of finding the absorption dipole at orientation (θ_a, ϕ_a) and the emission dipole at orientation (θ_e, ϕ_e) some time t later. Integrations are taken over all possible orientations of absorption and emission dipole, and over time. $d\Omega_a = \sin\theta_a\,d\theta_a\,d\phi_a$; $d\Omega_e = \sin\theta_e\,d\theta_e\,d\phi_e$. $P_a(\theta_a, \phi_a, \hat{\varepsilon})$ is the relative probability of absorbing a photon, given absorption dipole orientation (θ_a, ϕ_a) and electric field polarization $\hat{\varepsilon}$. $P_e(\theta_e, \phi_e, \hat{\alpha})$ is the relative probability of detecting an emitted photon, given emission dipole

orientation (θ_e, ϕ_e) and analyzer aligned along $\hat{\alpha}$. Expressions for $P_a(\theta_a, \phi_a, \hat{\varepsilon})$ and $P_e(\theta_e, \phi_e, \hat{\alpha})$ are given in Appendix A. The factor $(1/\tau)e^{-t/\tau}$ is a weighting function that expresses the normalized probability of emitting a photon at time t, after excitation, assuming a single fluorescence lifetime, τ. The infinite time integral is closely approximated when the measurement time is much greater than τ. K is a constant of proportionality that is independent of excitation/detector polarization and molecular orientation.

As described in the Applications Section 4 below, Ha et al. (1998, 1999a) have used a form of Eq. (6) to analyze SMFP data and obtained average azimuthal angles, extent of motion and rotational diffusion coefficients of their probes. It is useful to simplify Eq. (6) for the limiting cases of fast and slow wobble.

3.2.1. Fast wobble

In the case of fast wobble, the fluorophore fully samples a distribution of angles, within a region restricted by its local environment, over a time period much faster than the fluorescence lifetime. Therefore, all "memory" of the probe orientation (within its restricted range) at the instant of excitation is lost before the instant of emission. The orientation of the emission dipole, within its restricted range, at emission is independent of the orientation of the absorption dipole at excitation. This property implies that, $\rho(\theta_a, \phi_a, \theta_e, \phi_e, t)$ can be written as the product of two time-independent distribution functions, $\rho_{fa}(\theta_a, \phi_a)$ and $\rho_{fe}(\theta_e, \phi_e)$ which describe the independent probabilities of finding the absorption and emission dipoles in particular orientations. Eq. (6) then simplifies to the product of two terms that describe the absorption and emission separately

$$ {}_{\varepsilon}I_{\alpha} = K\left[\int \rho_{fa}(\theta_a, \phi_a)P_a(\theta_a, \phi_a, \hat{\varepsilon})d\Omega_a\right]\left[\int \rho_{fe}(\theta_e, \phi_e)P_e(\theta_e, \phi_e, \hat{\alpha})d\Omega_e\right]. \tag{7} $$

Polarization ratios calculated from measurements taken with different values of $\hat{\varepsilon}$ and/or $\hat{\alpha}$ may be considered as in the stationary molecule case. For a set of intensity measurements that vary only in excitation polarization, $\hat{\varepsilon}$, the second integral term in Eq. (7) will be constant. Therefore, this term will cancel when an absorption polarization ratio is calculated from these intensities. Analogously, an emission polarization ratio will be independent of the first integral term in Eq. (7). Therefore, as in the case of a static fluorophore, absorption polarization ratios are independent of the detection polarization, and emission polarization ratios are independent of the excitation polarization. For example, if a molecule is alternately excited with x and y polarized light, the resulting absorption polarization ratio, using expressions for $P_a(\theta_a, \phi_a)$ and $P_e(\theta_e, \phi_e)$ given in the Appendix, is

$$ Q = \frac{{}_yI_{\alpha} - {}_xI_{\alpha}}{{}_yI_{\alpha} + {}_xI_{\alpha}} = \frac{\int \rho_{fa}(\theta_a, \phi_a)\sin^2\theta_a\left(\sin^2\phi_a - \cos^2\phi_a\right)d\Omega_a}{\int \rho_{fa}(\theta_a, \phi_a)\sin^2\theta_a d\Omega_a}. \tag{8} $$

Note that this equation is similar to that for the static case (Eq. (2)) except that the intensities are now averaged over the distribution of dipole orientations produced by the motion. Adding fast wobble reduces the range of possible polarization ratios, since the fluorophore is not aligned along any precise direction for the entire duration of a measurement. In effect, fast wobble, while still preserving the independence of the absorption and emission polarizations from each other, causes a reduction in the magnitude of polarization ratios.

3.2.2. Slow wobble

If the characteristic time scale of motion is much longer than the fluorescence lifetime, but still shorter than the measurement time, then the molecule is effectively static between corresponding absorption and emission events. Therefore, during the time between absorption and emission (i.e. over the time integral of Eq. (6)) $\rho(\theta_a, \phi_a, \theta_e, \phi_e, t)$ is constant and may be approximated by the time-independent probability, $\rho_s(\theta_a, \phi_a, \theta_e, \phi_e)$, of finding the absorption and emission dipoles oriented in the directions (θ_a, ϕ_a) and (θ_e, ϕ_e), respectively. Eq. (6) then simplifies to

$$ {}_{\varepsilon}I_{\alpha} = K \iint \rho_s(\theta_a, \phi_a, \theta_e, \phi_e) P_a(\theta_a, \phi_a, \hat{\varepsilon}) P_e(\theta_e, \phi_e, \hat{\alpha}) d\Omega_a d\Omega_e. \tag{9} $$

In this case the integrations over $d\Omega_a$ and $d\Omega_e$ are not separable. Therefore, when absorption polarization ratios are calculated, terms with $P_e(\theta_e, \phi_e, \hat{\alpha})$ do not cancel as in the static and fast wobble cases. Analogously, when emission polarization ratios are calculated, terms with $P_a(\theta_a, \phi_a, \hat{\varepsilon})$ do not cancel. In contrast to the static fluorophore and fast wobble cases (Eqs. (2) and (8)), the absorption polarization ratios for slow wobble depend on the detector polarization, and the emission polarization ratios depend on the excitation polarization. This property, and Eq. (9), also describe fluorescence polarization data for a static distribution of many fluorophores. Slow wobble thus makes a single molecule appear to have polarization properties similar to those of a bulk sample.

Again, taking x and y polarized excitations as an example, the absorption polarization ratio, analogous to that in Eqs. (2) and (8), is given by

$$ \begin{aligned} Q_{\alpha} &= \frac{{}_{y}I_{\alpha} - {}_{x}I_{\alpha}}{{}_{y}I_{\alpha} + {}_{x}I_{\alpha}} \\ &= \frac{\iint \rho_s(\theta_a, \phi_a, \theta_e, \phi_e)\left(\sin^2\theta_a\right)\left(\sin^2\phi_a - \cos^2\phi_a\right) P_e(\theta_e, \phi_e, \hat{\alpha}) d\Omega_a \, d\Omega_e}{\iint \rho_s(\theta_a, \phi_a, \theta_e, \phi_e)\left(\sin^2\theta_a\right) P_e(\theta_e, \phi_e, \hat{\alpha}) \, d\Omega_a \, d\Omega_e}. \end{aligned} \tag{10} $$

Note that here, the subscript, α, has been added to the polarization ratio, Q. This is necessary since, as explained above, the value of this *absorption* polarization ratio, is dependent on the orientation, $\hat{\alpha}$, of the *detector* polarizer, which determines $P_e(\theta_e, \phi_e, \hat{\alpha})$. Q_x measured from x-polarized detection does not equal Q_y measured from y-polarized detection. A simple check, then, to evaluate the extent of slow motion in a single molecule system, which follows from this analysis, is to measure a pair of absorption or emission polarization ratios (e.g. $Q_x$and Q_y or ${}_{x}P$ and ${}_{y}P$). The pair will differ only if slow wobble is present.

3.3. Measurement of the axial angle, θ

Wide-field epiillumination and laser spot-confocal excitation cannot readily be used to determine the axial angle of the absorption transition dipole moment, θ_a. The difficulty is that for an excitation laser beam propagating along the optical axis of the microscope, the polarization at the center of the beam is in the plane of the microscope stage (Axelrod, 1989b). The intensities in Eqs. (1) and (3) are sensitive to $\sin^2\theta_a$ but they are also proportional to a number of other physical parameters, such as intensity of the laser, absorption cross section, etc. Because these factors are difficult to quantify, θ_a cannot be inferred directly. The excitation polarization ratio (Eq. (2)) is completely independent of θ_a. The use of a high numerical aperture objective results in

some dependence of emission polarization ratios on θ_e, as shown in Eq. (5). Introduction of motion may also introduce some θ_a or θ_e dependence of absorption and emission polarization ratios. However with axially propagating excitation, the sensitivities of polarized fluorescence ratios to θ_a and θ_e are low.

To get around this problem, some studies have made use of specialized fluorophores with multiple degenerate transition dipole moments distributed isotropically in a plane perpendicular to a symmetry axis (Bopp et al., 1997, 1999; Empedocles et al., 1999). With these unusual fluorophores, both axial and azimuthal angles of the symmetry axis can be determined with wide-field epiillumination or spot-confocal excitation.

A more direct solution, that applies to conventional fluorophores with linear, non-degenerate, transition dipole moments, is to utilize excitation with a large component of electric field along the optical axis of the microscope (i.e. along the z-axis; Betzig and Chichester, 1993; Dickson et al., 1998; Forkey et al., 1999). The evanescent waves generated by total internal reflection and near-field scanning optical probes have polarization with large z-components. For a static molecule excited with a z-polarized electric field, the intensity expression, analogous to Eq. (1) is

$$ {}_zI \propto \cos^2\theta_a \tag{11}$$

and an absorption polarization ratio, analogous to that in Eq. (2) can be calculated. For example

$$Q' \equiv \frac{{}_zI - {}_xI}{{}_zI + {}_xI} = \frac{\cos^2\theta_a - \sin^2\theta_a\cos^2\phi_a}{\cos^2\theta_a + \sin^2\theta_a\cos^2\phi_a} = \frac{1 - \tan^2\theta_a\cos^2\phi_a}{1 + \tan^2\theta_a\cos^2\phi_a}. \tag{12}$$

This polarization ratio is dependent on the axial angle, θ_a, and, therefore, may be used in conjunction with another measurement, such as Q in Eq. (2) to determine both polar angles of the absorption dipole.

The evanescent wave generated by total internal reflection is an excellent source for this type of measurement. Expressions for the evanescent wave electric fields generated by total internal reflection of p- and s-polarized laser beams (see Section 2.2.2) at the interface between a microscope slide and an aqueous sample chamber are (Axelrod et al., 1984; Thompson et al., 1984):

$$\mathbf{E}_p = \begin{bmatrix} \hat{x}2A_p\cos\theta_i\sin\delta_p\exp\left(-i\frac{\pi}{2}\right)\exp(-i\delta_p) \\ +\hat{z}2A_p(1/\xi^2)\sin\theta_i\cos\delta_p\exp(-i\delta_p) \end{bmatrix}\exp(-z/d)\exp(-i(\omega t - n_1k_0x\sin\theta_i))$$

$$\mathbf{E}_s = [\hat{y}2A_s\cos\delta_s\exp(-i\delta_s)]\exp(-z/d)\exp(-i(\omega t - n_1k_0x\sin\theta_i))$$

$$\xi = \frac{n_2}{n_1}, \quad d = \left(n_1k_0\sqrt{\sin^2\theta_i - \xi^2}\right)^{-1}, \quad \theta_i > \theta_c \equiv \sin^{-1}(\xi), \tag{13}$$

$$\delta_p = \tan^{-1}\left[\frac{\sqrt{\sin^2\theta_i - \xi^2}}{\xi^2\cos\theta_i}\right], \quad \delta_s = \tan^{-1}\left[\frac{\sqrt{\sin^2\theta_i - \xi^2}}{\cos\theta_i}\right],$$

where the actual electric fields are given by the real parts of the expressions for $\mathbf{E}_p$ and $\mathbf{E}_s$. These equations assume that the scattering plane is the x–z plane (see Fig. 4b). A_p and A_s are the electric field amplitudes of the p- and s-wave laser beams, respectively. θ_i is the angle of the incident laser beam relative to the direction normal to the interface and θ_c is the critical angle,

beyond which total internal reflection occurs. n_1 is the index of refraction on the side of the interface with the propagating laser beam, and n_2 is the refractive index on the side of the interface with the evanescent wave. d represents the $1/e$ decay distance of the amplitude of the evanescent wave. ω is the radial frequency, and k_o the vacuum wave number of the excitation laser beam.

For a quartz slide ($n_1 = 1.46$)/water ($n_2 = 1.33$) interface, total internal reflection of an argon ion laser beam with wavelength 514 nm occurs for incident angles greater than the critical angle of $\sim 66^\circ$. For an incident angle, θ_i, of 70° an evanescent wave is generated with amplitude decay distance, d, of 240 nm (intensity decay distance, $d/2 = 120$ nm). The evanescent wave generated by an s-polarized incident beam is linearly polarized along the y-direction and has intensity $|\mathbf{E}_s \cdot \hat{y}|^2 = 2.7A_s^2$ at the slide surface; the evanescent wave generated by a p-polarized incident beam is elliptically polarized in the x–z plane with $\left|\mathbf{E}_p \cdot \hat{z}\right|^2 = 3.1A_p^2$ and $\left|\mathbf{E}_p \cdot \hat{x}\right|^2 = 0.2A_p^2$ at the slide surface. For the p-generated wave, the component of the electric field along the x-direction can easily be taken into account in expressions for the polarization ratios. However, the x-component of the electric field is so much smaller than the z-component, that the excitation probability is dominated by the z-component of the absorption dipole. This makes total internal reflection a particularly useful excitation source for determining the full three-dimensional orientation of single fluorescent molecules.

4. Applications

The studies summarized in this section make use of the experimental and analytical methods described above. In contrast to many of the early experiments, those described here apply to functioning biophysical systems in aqueous media.

Using a laser spot-confocal apparatus, Ha et al. (1996) determined the orientation of single DNA-bond fluorophore dipoles projected onto the x–y plane. With data averaged over ~ 4 s they achieved an impressive angular resolution of 0.2°. The data enabled unambiguous differentiation between molecular rotations, and spectral jumps or transitions to non-fluorescent states. While these initial measurements were made at a slide/air interface, subsequent studies incorporated an aqueous medium. Ha et al. (1998) resolved the orientation of the transition dipole moment of single Texas Red probes covalently linked to short single-stranded DNA (ssDNA) bound to silanized glass. The DNA tethered the fluorophore in the aqueous solution, close to the slide while allowing rotation. The linear polarization angle of the fluorescence excitation was swept through a 120° range in the plane of the microscope stage during a period of ~ 50 ms, and the fluorescence emission was resolved into orthogonal components by a polarizing beam splitter. Averages over several angle scans (Fig. 6) were analyzed using a limited diffusion model (similar to Eq. (6) above) and assuming that the absorption and emission dipoles were colinear. Analysis of the experiments yielded the average orientation and extent of motion projected onto the x–y plane, as well as the rotational diffusion rate. Individual fluorophores were observed to "jump" repeatedly from a rotating state to a fixed orientation and vice versa, suggesting that individual probes repeatedly adsorbed to the glass substrate and were released from it. Some molecules which exhibited multiple jumps returned to fixed orientations, indicating preferential binding sites on the substrate. Further experiments with DNA may reveal new aspects

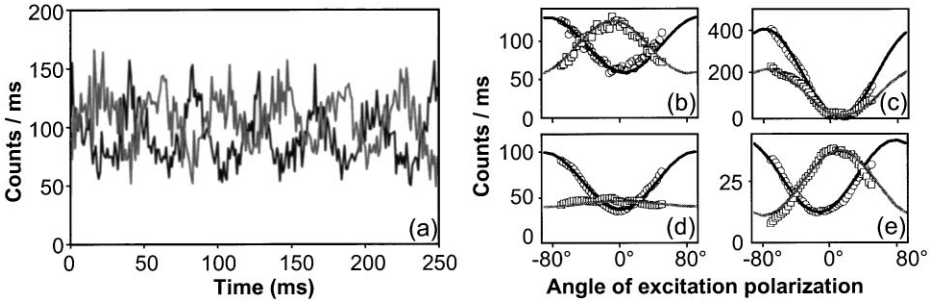

Fig. 6. SMFP experiments with high angular resolution. Fluorescence from single Texas Red molecules was excited by polarized spot-confocal excitation. The linear polarization of the excitation beam was repeatedly rotated through 120° in the x–y plane. Fluorescence was split into its two orthogonal polarization components by a polarizing beam splitter. (a) Raw data shows the two intensities (indicated by black and gray traces) changing with excitation polarization. The orthogonally polarized signals are out of phase as expected for a freely rotating molecule. (b–e) Time-averaged data (symbols) and fitted curves based on a limited rotational diffusion model. Amplitudes and relative phases indicate mean probe orientation and degree of rotational freedom. (Modified with permission from Ha et al., 1998.).

of its physical properties and its interactions with other macromolecules. Using a similar technique, structural changes of staphylococcal nuclease upon binding of an inhibitor, have also been detected (Ha et al., 1999b).

Schmidt et al. (1995) interrogated motions of individual tetramethylrhodamine (TMR)-labeled 1-2-dihexadecanoyl-*sn*-glycero-3-phosphoethanolamine (DHPE) molecules in bilayer membranes. They demonstrated tracking, with 10 ms time resolution, of single DHPE molecules diffusing in 1-palmitoyl-2-oleoyl-*sn*-glycero-3-phosphocholine (POPC) membranes. In further experiments, SMFP was used to detect rotational mobility (Schütz et al., 1997). Polarization of the laser excitation beam was switched at 30 Hz, by an electro-optic modulator, between two discrete orientations in the sample plane and absorption polarization ratios (Q given in Eqs. (2), (8) and (10)) were calculated. For TMR-labeled DHPE in POPC membranes, the average absolute value of Q ($|\bar{Q}|$) was 0.14. This value indicates virtually free rotational mobility on the submillisecond time scale. In contrast, DHPE embedded in a solid membrane composed of 1,2-dipalmitoyl-*sn*-glycero-3-phosphocholine (DPPC) gave $|\bar{Q}| = 0.66$, consistent with immobile fluorophores randomly oriented in the plane of the bilayer. Similar experiments with TMR- and Cy7-labeled lipid molecules in DPPC membranes allowed sequential measurements of orientation to determine the trajectory of slow motion (Harms et al., 1999). The extent of rotational mobility of the probe molecules agrees with earlier studies on bulk samples, thus indicating the potential for further investigations of individual macromolecules embedded in membranes.

The study of motor proteins is a natural application of SMFP because rotational motions are prevalent and in vitro assays of their function have already been well characterized (Scholey, 1993; Vallee, 1998). Sase et al. (1997) monitored the emission polarization ratio (P, Eq. (5)) from single TMR molecules conjugated to actin filaments. A 30 μm diameter region of the microscope slide was illuminated by circularly polarized wide-field epiillumination. As the filament was actively propelled by myosin, P oscillated between ca. –0.5 and +0.5 on a $\frac{1}{2}$ s timescale (Fig. 7). This experiment elegantly demonstrated rotation of the actin filament about its axis during translation. Because the observed pitch of rotation was more than 10-fold greater than that of the actin helix,

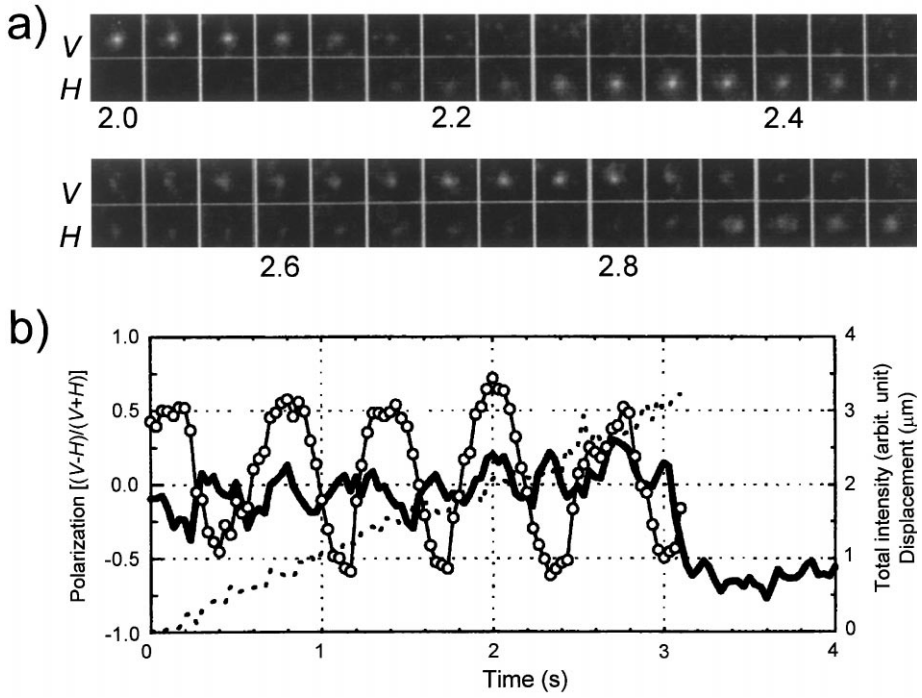

Fig. 7. Twisting of actin during translation in an in vitro actomyosin motility assay. (a) Polarized fluorescence images of an individual fluorophore attached to actin. The experiments used wide-field laser epiillumination with circularly polarized excitation, and the imaging system shown in Fig. 5b. V and H indicate vertically and horizontally polarized emission. Images were collected at 33-ms intervals. Alternating intensity levels in the two sequences of polarized images demonstrate that the actin filament rotated about its axis as it translated. (b) Total intensity of a spot during translocation ($I=V+H$, solid line); emission polarization ratio ($P=(V-H)/(V+H)$, open circles); displacement of the spot from its position at $t=0$ (broken line). (Reproduced with permission from Sase et al., "Axial rotation of sliding actin filaments revealed by single-fluorophore imaging", Proceedings of the National Academy of Sciences, USA 94, 5646–5650. Copyright (1994) National Academy of Sciences, USA).

these results indicate, in agreement with other studies, that the myosin is not rigidly constrained along the actin helix.

Warshaw et al. (1998) detected motions of TMR bound to myosin RLC (see Fig. 1c) in an in vitro motility assay. They excited the sample with circularly polarized light in a laser spot-confocal microscope, resolved emission from the probes into orthogonal components with a polarizing beam splitter and collected the fluorescence with two APDs at 1–10 ms time resolution. The intensity signals exhibited discrete, reversible transitions in the presence of ATP and actin. The duration of these events versus ATP concentration indicated that they were due to actomyosin association and dissociation during the force-generating enzymatic cycle. An emission polarization ratio similar to the P ratio (Eq. (5)) indicated extensive mobility of the RLC when the myosin was dissociated from actin and discrete orientations during association. The polarization ratio was constant during an event. This result indicates that attached 'pre-force' states are either disordered like detached ones or are occupied for a period shorter than the time resolution.

In a similar experiment, Quinlan et al. (1999) used myosin RLC labeled with bifunctional rhodamine (see Section 3.1.2 on Fluorescent Probes above and Fig. 2a). Evanescent waves with

polarizations along the y-axis and predominantly along the z-axis were generated by total internal reflection. The polarization of the input laser beam was switched by an electro-optic modulator at 50 Hz. The fluorescent emission was resolved into its components polarized along the x- and y-axis by a beam splitting prism and detected by two APDs (Forkey et al., 1999). As discussed above, this excitation scheme enables resolution of probe orientation in the x–y plane (ϕ) and along the z-axis (θ, Fig. 4c). Discrete changes of intensities were observed, often in opposite directions, indicating sudden changes of orientation and mobility of the RLC during actomyosin motility (Fig. 8). Coumarin probes attached to the actin filaments were also excited by an ultraviolet evanescent wave to select myosins colocalized with actin and to provide an angular reference axis. The bifunctional probe potentially enables protein orientation to be quantified

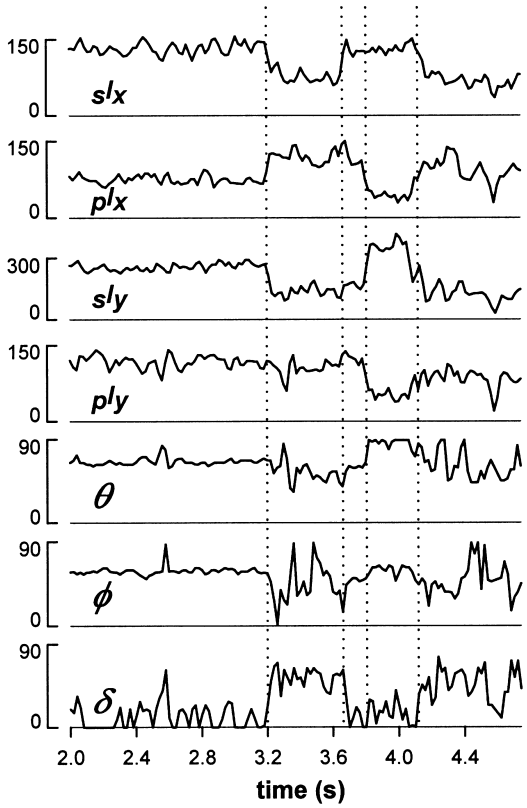

Fig. 8. Polarized fluorescence intensities and fitted orientation parameters for a single bifunctional rhodamine probe. The fluorophore was bound to the regulatory light chain of rabbit skeletal muscle myosin in an in vitro motility assay. The excitation source was an evanescent wave generated by total internal reflection (Fig. 4b). Time multiplexed s- and p-polarized excitation (see text), and two detector polarizations (Fig. 5a) yielded four independent intensities: ${}_{s}I_{x}$, ${}_{p}I_{x}$, ${}_{s}I_{y}$, and ${}_{p}I_{y}$. Intensities are plotted as number of photons detected during two 10 ms periods with constant excitation polarization. Axial angle (θ), azimuthal angle (ϕ) and a mobility parameter (δ) are given in degrees. θ is the half-angle of a cone describing the extent of mobility on the 'slow wobble' time scale (see Section 3). Time is indicated in seconds relative to the start of excitation. Values of the measured parameters between 0 and 2 s were approximately constant. The abrupt changes in intensities, highlighted by the dotted lines, indicate changes in orientation and extent of mobility of the myosin light chain domain.

from the probe orientation in relation to this reference axis as was reported in bulk experiments with the actomyosin system (Corrie et al., 1999).

A third research group applying SMFP to myosin-based motility used evanescent wave excitation through a high numerical aperture microscope objective (Saito et al., 1997). In this case, the propagation direction of a totally reflected, s-polarized incident beam was switched between x–z and y–z scattering planes by alternating (at 10 Hz) its position at the objective back focal plane. These two excitation modes generated evanescent wave polarizations along the y- and x-axis, respectively. Total fluorescence intensity was monitored from single probe molecules bound to the motor domain of myosin (see Fig. 1c) or to the RLC. Absorption polarization ratios indicated that fluorophores bound to the motor domain were less mobile than those bound to the RLC.

While the studies described thus far all made use of extrinsic fluorophores attached to the biological molecule of interest, intrinsic fluorophores may also be used. This was demonstrated by Bopp et al. (1997) who measured the molecular orientation of the light harvesting complex (LH-2) from the purple bacterium, *Rhodopseudomonas acidophila*, using a spot-confocal microscope. Instead of a discrete absorption dipole as in the previously discussed systems, LH-2 contains a set of fluorophores arranged around a molecular symmetry axis. Measurements by Bopp et al. using two orthogonal excitation polarizations in the plane of the microscope slide, were consistent with a homogeneous surface distribution of cyllindrically symmetric LH-2 complexes with their axes tilted 20–30° relative to the substrate normal. More recently, the excitation polarization was swept through a range of orientations on a time scale faster than 100 ms (Bopp et al., 1999). These measurements indicated that the molecules are not circularly symmetric, but can be described as elliptic absorbers. Discrete jumps in ellipticity and orientation of the major axes found in the 10 s time domain indicated structural deformations.

5. Conclusions

The technology, components and analytical tools are now readily available to perform biologically relevant SMFP experiments. Nevertheless, the method has not yet been widely applied partly because it is new, but also because significant hurdles limit the preparation and characterization of the experimental materials. Functioning samples that can be integrated into SMFP instruments have been designed for several macromolecular systems. Most of these involve attachment of the enzyme complex or lipid bilayer to the surface of the microscope slide necessitating careful evaluation of functional integrity under these conditions. Measurements of fluorescence polarization from bound probes reveal the mobility of the labeled component in various occupied states and kinetics of transitions between them. Quantifying domain orientation from the probe angles, however, requires knowledge of the local probe orientation within the macromolecule. Determination of these angles has been accomplished in only a few cases. Availability of new probes capable of labeling proteins with predetermined orientation, improved methods for attachment without compromising activity and innovations in the assay methods should promote application of SMFP to studies of many more biophysical systems.

Further development of SMFP will increase the accessible information. For example, the use of multiple, spectrally distinct fluorophores would allow simultaneous orientation measurements

on several domains. Also, continued advancement of video cameras may enhance polarization measurements on spatially separated molecules. Integration of SMFP with other single molecule techniques will enable direct correlation of structural changes with other processes. Combination with optical traps would enable correlation between structural changes and mechanical events such as force production or movement. Combination of SMFP with detection of ligand binding and dissociation would provide the timing of conformational changes relative to these chemical reactions. With continued development and implementation, SMFP is expected to play a major role in elucidating the dynamic relationships between structural changes in macromolecular machines and their functional output.

Acknowledgements

This work was supported by the NIH, MDA, AHA and HHMI. We thank Drs. John E. T. Corrie, Enrique M. De La Cruz, Carol J. Deutsch, Dennis E. Discher, Uulke van der Heide, Michael Ostap, Brian M. Salzberg and Mr. Francesco Vanzi for helpful discussions and comments on the manuscript.

Appendix A. Dependence of polarized fluorescence intensity on molecular orientation

In this appendix, equations are presented that show the dependence on molecular orientation of single-molecule polarized fluorescence intensities. The molecule is presumed to have well defined, linear, absorption and emission transition dipole moments. The fluorescence from a single molecule on a microscope slide is collected and collimated by a microscope objective having a high numerical aperture. The right handed Cartesian coordinate system, described by the unit vectors $\hat{x}, \hat{y}$ and $\hat{z}$ (Fig. 4c), has its origin on the slide surface. The positive z-axis coincides with the optical axis of the microscope, and points toward the objective.

A.1. Excitation of a single fluorophore

The oscillating electric field **E** at a given point for any of the excitation schemes used in single-molecule experiments may be written in the form

$$\mathbf{E} = E\hat{\varepsilon}\mathrm{e}^{-\mathrm{i}\omega t},$$

$$\hat{\varepsilon} = \left[\hat{x}\,\varepsilon_x \mathrm{e}^{-\mathrm{i}\delta_x} + \hat{y}\varepsilon_y \mathrm{e}^{-\mathrm{i}\delta_y} + \hat{z}\varepsilon_z \mathrm{e}^{-\mathrm{i}\delta_z}\right], \tag{A.1}$$

where the actual electric field is given by the real part of this complex expression. Here, E is the magnitude of the electric field, ω is the radial frequency of the field, and t is time. $\hat{\varepsilon}$ describes the polarization. ε_j and δ_j represent the relative magnitude and phase, respectively, of the jth component of the electric field and the ε_j values have been normalized so that $|\hat{\varepsilon}| = \sqrt{\varepsilon_x^2 + \varepsilon_y^2 + \varepsilon_z^2} = 1$.

For an individual molecule, the orientation of its absorption transition dipole moment may be described either by axial and azimuthal polar angles, θ_a and ϕ_a, respectively, or equivalently

by the unit vector $\hat{\mu}_a = \hat{x}\mu_{ax} + \hat{y}\mu_{ay} + \hat{z}\mu_{az}$, where $\mu_{ax} = \sin\theta_a \cos\phi_a$, $\mu_{ay} = \sin\theta_a \sin\phi_a$, and $\mu_{az} = \cos\theta_a$. The probability per unit time of exciting this molecule is proportional to the square of the magnitude of the projection of the electric field along the direction of the absorption dipole. In particular, the dependence of the excitation probability on the electric field polarization, $\hat{\varepsilon}$, and molecular orientation, $\hat{\mu}_a$, is given by $P_a(\hat{\mu}_a, \hat{\varepsilon})$ which is defined as

$$\begin{aligned} P_a(\hat{\mu}_a, \hat{\varepsilon}) &\equiv |\hat{\mu}_a \cdot \hat{\varepsilon}|^2 \\ &= \left(\varepsilon_x \mu_{ax} \cos\delta_x + \varepsilon_y \mu_{ay} \cos\delta_y + \varepsilon_z \mu_{az} \cos\delta_z\right)^2 \\ &\quad + \left(\varepsilon_x \mu_{ax} \sin\delta_x + \varepsilon_y \mu_{ay} \sin\delta_y + \varepsilon_z \mu_{az} \sin\delta_z\right)^2, \end{aligned} \tag{A.2}$$

where the dependence of μ_{ax}, μ_{ay} and μ_{az} on (θ_a, ϕ_a) has been given above.

Eq. (A.2) may often be reduced to a relatively simple expression depending on the particular mode of excitation. A number of examples are:

Epifluorescence (wide-field or spot-confocal) with electric field linearly polarized along the x-axis:

$$\varepsilon_x = 1,\ \varepsilon_y = \varepsilon_z = 0,$$

$$P_a(\hat{\mu}_a, \hat{\varepsilon}) = \mu_{ax}^2 = \sin^2\theta_a \cos^2\phi_a;$$

Epifluorescence with electric field linearly polarized along the y-axis:

$$\varepsilon_y = 1, \quad \varepsilon_x = \varepsilon_z = 0,$$

$$P_a(\hat{\mu}_a, \hat{\varepsilon}) = \mu_{ay}^2 = \sin^2\theta_a \sin^2\phi_a;$$

Epifluorescence with electric field linearly polarized in the x–y plane and making an angle ζ relative to the x-axis:

$$\varepsilon_x = \cos\zeta, \quad \varepsilon_y = \sin\zeta, \quad \varepsilon_z = 0, \quad \delta_x = \delta_y,$$

$$\begin{aligned} P_a(\hat{\mu}_a, \hat{\varepsilon}) &= \left(\mu_{ax}\cos\zeta + \mu_{ay}\sin\zeta\right)^2 \\ &= (\sin\theta_a \cos\phi_a \cos\zeta + \sin\theta_a \sin\phi_a \sin\zeta)^2 = \sin^2\theta_a \cos^2(\zeta - \phi_a); \end{aligned}$$

Epifluorescence with a circularly polarized electric field in the x–y plane:

$$\varepsilon_x = \varepsilon_y = 1/\sqrt{2}, \quad \varepsilon_z = 0, \quad \delta_y = \delta_x \pm \pi/2$$

$$P_a(\hat{\mu}_a, \hat{\varepsilon}) = \tfrac{1}{2}\left(\mu_{ax}^2 + \mu_{ay}^2\right) = \tfrac{1}{2}\sin^2\theta_a;$$

Evanescent wave generated by total internal reflection of an s-polarized excitation laser beam propagating in the x–z plane (see Section 3.3):

$$\varepsilon_x = \varepsilon_z = 0, \quad \varepsilon_y = 1,$$

$$P_a(\hat{\mu}_a, \hat{\varepsilon}) = \mu_{ay}^2 = \sin^2\theta_a \sin^2\phi_a;$$

Evanescent wave generated by total internal reflection of a p-polarized excitation laser beam propagating in the x–z plane (see Section 3.3):

$$\varepsilon_x = \sqrt{\kappa},\ \varepsilon_y = 0,\ \varepsilon_z = \sqrt{1-\kappa},\ \delta_x = \delta_z + \pi/2\ \ (0 < \kappa \ll 1).$$

$$P_a(\hat{\mu}_a,\ \hat{\varepsilon}) = \kappa\mu_{ax}^2 + (1-\kappa)\mu_{az}^2 = \kappa \sin^2\theta_a \cos^2\phi_a + (1-\kappa)\cos^2\theta_a.$$

A.2. Fluorescence from a single fluorophore

When a molecule fluoresces, the probability of any emitted photon propagating in some direction, $\hat{k}$, is proportional to the square of the magnitude of the induced electric field propagating in that direction. At locations much farther from the molecule than the wavelength (i.e. far field), this electric field is given by

$$\mathbf{E}_{\text{dipole}} = K'\left[\hat{\mu}_e - \left(\hat{\mu}_e \cdot \hat{k}\right)\hat{k}\right]e^{-i\omega t}, \tag{A.3}$$

where $\hat{\mu}_e = \hat{x}\mu_{ex} + \hat{y}\mu_{ey} + \hat{z}\mu_{ez}$ is a unit vector in the direction of the molecule's emission transition dipole moment (Born and Wolf, 1964, Section 2.2). K' is a scale factor that is independent of molecular orientation but depends on other physical parameters such as excitation rate and fluorescence quantum efficiency. The magnitude squared of this field is proportional to $1 - (\hat{\mu}_e \cdot \hat{k})^2$ which equals $\sin^2\chi$, where χ is the angle between $\hat{\mu}_e$, and the propagation direction, $\hat{k}$.

Because the fluorescence in this far-field region is a transverse propagating wave, it is polarized in the plane perpendicular to $\hat{k}$. The intensity of the fluorescence with polarization along some specific direction, $\hat{A}$, perpendicular to $\hat{k}$ (i.e. $\hat{A} \cdot \hat{k} = 0$), is proportional to the square of the projection of $\mathbf{E}_{\text{dipole}}$ onto $\hat{A}$, as given by

$$P'_e(\hat{\mu}_e,\ \hat{A}) \equiv \left|\left[\hat{\mu}_e - \left(\hat{\mu}_e \cdot \hat{k}\right)\hat{k}\right] \cdot \hat{A}\right|^2 = \left|\hat{\mu}_e \cdot \hat{A}\right|^2. \tag{A.4}$$

For a system that uses a high numerical aperture objective lens, the polarization analyzer is placed after the objective, where the collected light is approximately collimated along the z-axis. Integrating Eq. (A.4) over all $\hat{k}$ directions subtended by the objective, and taking into account the collimation of the fluorescence, yields the following probability function for detecting a photon after the objective, with the analyzer along $\hat{\alpha}$, in the x–y plane:

$$P_e(\hat{\mu}_e,\ \hat{\alpha}) = C_1\left(\mu_{ex}\cos\eta + \mu_{ey}\sin\eta\right)^2 + C_2\left(\mu_{ex}\sin\eta - \mu_{ey}\cos\eta\right)^2 + C_3\mu_{ez}^2, \tag{A.5}$$

where η is the angle between $\hat{\alpha}$ and the x-axis, defined to be positive for rotation from the positive x-axis towards the positive y-axis. The formulas for C_1, C_2 and C_3 that express mixing of polarizations between the orthogonal directions due to the high numerical aperture have been derived elsewhere for use in the analysis of polarization microscopy measurements on bulk samples (Axelrod, 1989b):

$$C_1 = (1/8)\left[5 - 3\cos(\delta_c) - \cos^2(\delta_c) - \cos^3(\delta_c)\right]\left[1 - \cos(\delta_c)\right]^{-1},$$

$$C_2 = (1/24)\left[1 - 3\cos(\delta_c) + 3\cos^2(\delta_c) - \cos^3(\delta_c)\right]\left[1 - \cos(\delta_c)\right]^{-1},$$

$$C_3 = (1/6)\left[2 - 3\cos(\delta_c) + \cos^3(\delta_c)\right]\left[1 - \cos(\delta_c)\right]^{-1}. \tag{A.6}$$

Here, δ_c is the half-angle of the collection cone subtended by the objective at the sample and is given by $\delta_c = \sin^{-1}(NA/n)$. NA is the numerical aperture of the objective, and n is the index of refraction of the medium containing the sample. These formulas for C_1, C_2 and C_3 do not include effects due to reflections of emitted light at water/slide/oil interfaces or effects of non-propagating components of the dipole radiation (i.e. near-field emission). These effects have been discussed by Hellen and Axelrod (1987).

A polarization analyzer after the objective will commonly split the fluorescence into components with polarization parallel to the x- and y-axis. For these cases, Eq. (A.5) simplifies to

$$P_e(\hat{\mu}_e, \hat{x}) = C_1\mu_{ex}^2 + C_2\mu_{ey}^2 + C_3\mu_{ez}^2 = C_1 \sin^2\theta_e \cos^2\phi_e + C_2 \sin^2\theta_e \sin^2\phi_e + C_3 \cos^2\theta_e,$$
$$P_e(\hat{\mu}_e, \hat{y}) = C_2\mu_{ex}^2 + C_1\mu_{ey}^2 + C_3\mu_{ez}^2 = C_2 \sin^2\theta_e \cos^2\phi_e + C_1 \sin^2\theta_e \sin^2\phi_e + C_3 \cos^2\theta_e. \quad (A.7)$$

where θ_e and ϕ_e are axial and azimuthal polar angles, respectively, of the emission dipole.

Combining the expressions for the relative absorption and detection probabilities yields a general equation for the expected dependence on molecular orientation, of fluorescence intensities from a single non-rotating molecule:

$$I(\hat{\mu}_a, \hat{\mu}_e, \hat{\varepsilon}, \hat{\alpha}) = K'' P_a(\hat{\mu}_a, \hat{\varepsilon}) P_e(\hat{\mu}_e, \hat{\alpha}), \quad (A.8)$$

where K'' is a constant, independent of $\hat{\mu}_a$, $\hat{\mu}_e$, $\hat{\varepsilon}$ and $\hat{\alpha}$. $P_a(\hat{\mu}_a, \hat{\varepsilon})$ is given in Eq. (A.2) (or the expressions that follow it for specific types of excitation) and $P_e(\hat{\mu}_e, \hat{\alpha})$ is given in Eq. (A.5) (or A.7).

References

Ambrose, W.P., Goodwin, P.M., Martin, J.C., Keller, R.A., 1994. Single molecule detection and photochemistry on a surface using near-field optical excitation. Phys. Rev. Lett. 72, 160–163.

Ambrose, W.P., Goodwin, P.M., Nolan, J.P., 1999. Single-molecule detection with total internal reflection excitation: comparing signal-to-background and total signals in different geometries. Cytometry 36, 224–231.

Ambrose, W.P., Moerner, W.E., 1991. Fluorescence spectroscopy and spectral diffusion of single impurity molecules in a crystal. Nature 349, 225–227.

Axelrod, D., 1989a. Total internal reflection fluorescence microscopy. Methods Cell Biol. 30, 245–270.

Axelrod, D., 1989b. Fluorescence polarization microscopy. Methods Cell Biol. 30, 333–352.

Axelrod, D., Burghardt, T.P., Thompson, N.L., 1984. Total internal reflection fluorescence. Annu. Rev. Biophys. Bioeng. 13, 247–268.

Barak, L.S., Webb, W.W., 1981. Fluorescent low density lipoprotein for observation of dynamics of individual receptor complexes on cultured human fibroblasts. J. Cell Biol. 90, 595–604.

Basché, T., Moerner, W.E., Orrit, M., Wild, U.P., 1997. Single-Molecule Optical Detection, Imaging and Spectroscopy. VCH Publishers, Inc., New York.

Betzig, E., Chichester, R.J., 1993. Single molecules observed by near-field scanning optical microscopy. Science 262, 1422–1425.

Betzig, E., Trautman, J.K., 1992. Near-field optics: microscopy, spectroscopy, and surface modification beyond the diffraction limit. Science 257, 189–195.

Bopp, M.A., Jia, Y., Li, L., Cogdell, R.J., Hochstrasser, R.M., 1997. Fluorescence and photobleaching dynamics of single light-harvesting complexes. Proc. Natl. Acad. Sci. USA 94, 10630–10635.

Bopp, M.A., Sytnik, A., Howard, T.D., Cogdell, R.J., Hochstrasser, R.M., 1999. The dynamics of structural deformations of immobilized single light-harvesting complexes. Proc. Natl. Acad. Sci. USA 96, 11271–11276.

Born, M., Wolf, E., 1964. Principles of Optics: Electromagnetic Theory of Propagation, Interference and Diffraction of Light, 2nd Edition (Section: 2.2.3). MacMillan, New York, pp. 81–84.

Boyer, P.D., 1997. The ATP synthase — a splendid molecular machine. Annu. Rev. Biochem. 66, 717–749.

Cantor, C.R., Schimmel, P.R., 1980. Biophysical Chemistry. Part II: Techniques for the Study of Biological Structure and Function. W.H. Freeman and Company, New York.

Carniglia, C.K., Mandel, L., Drexhage, K.H., 1972. Absorption and emission of evanescent photons. J. Opt. Soc. Am. 62, 479–486.

Chen, R.F., Bowman, R.L., 1965. Fluorescence polarization: measurement with ultraviolet-polarizing filters in a spectrophotofluorometer. Science 147, 729–732.

Clark, B.F.C., Thirup, S., Kjeldgaard, M., Nyborg, J., 1999. Structural information for explaining the molecular mechanism of protein biosynthesis. FEBS Lett. 452, 41–46.

Conibear, P.B., Kuhlman, P.A., Bagshaw, C.R., 1998. Measurement of ATPase activites of myosin at the level of tracks and single molecules. Adv. Exp. Med. Biol. 453, 15–26.

Corrie, J.E.T., Brandmeier, B.D., Ferguson, R.E., Trentham, D.R., Kendrick-Jones, J., Hopkins, S.C., van der Heide, U.A., Goldman, Y.E., Sabido-David, C., Dale, R.E., Criddle, S., Irving, M., 1999. Dynamic measurement of myosin light-chain-domain tilt and twist in muscle contraction. Nature 400, 425–430.

Corrie, J.E.T., Craik, J.S., Munasinghe, V.R.N., 1998. A homobifunctional rhodamine for labeling proteins with defined orientations of a fluorophore. Bioconjugate Chem. 9, 160–167.

Cubitt, A.B., Heim, R., Adams, S.R., Boyd, A.E., Gross, L.A., Tsien, R.Y., 1995. Understanding, improving and using green fluorescent proteins. TiBS 20, 448–455.

Dale, R.E., 1988. Some aspects of excited-state probe emission spectroscopy for structure and dynamics of model and biological membranes. In: Samori', B., Thulstrup, E.W. (Eds.), Polarized Spectroscopy of Ordered Systems. Kluwer Academic Publishers, Dordrecht, The Netherlands, pp. 491–567.

Dautet, H., Deschamps, P., Dion, B., MacGregor, A.D., MacSween, D., McIntyre, R.J., Trottier, C., Webb, P.P., 1993. Photon counting techniques with silicon avalanche photodiodes. Appl. Opt. 32, 3894–3900.

Dickson, R.M., Cubitt, A.B., Tsien, R.Y., Moerner, W.E., 1997. On/off blinking and switching behaviour of single molecules of green fluorescent protein. Nature 388, 355–358.

Dickson, R.M., Norris, D.J., Moerner, W.E., 1998. Simultaneous imaging of individual molecules aligned both parallel and perpendicular to the optic axis. Phys. Rev. Lett. 81, 5322–5325.

Dickson, R.M., Norris, D.J., Tzeng, Y.-L., Moerner, W.E., 1996. Three-dimensional imaging of single molecules solvated in pores of poly(acrylamide) gels. Science 274, 966–969.

Dominguez, R., Freyzon, Y., Trybus, K.M., Cohen, C., 1998. Crystal structure of a vertebrate smooth muscle myosin motor domain and its complex with the essential light chain: visualization of the pre-power stroke state. Cell 94, 559–571.

Doyle, D.A., Cabral, J.M., Pfuetzner, R.A., Kuo, A., Gulbis, J.M., Cohen, S.L., Chait, B.T., MacKinnon, R., 1998. The structure of the potassium channel: molecular basis of K^+ conduction and selectivity. Science 280, 69–77.

Dürig, U., Pohl, D.W., Rohner, F., 1986. Near-field optical-scanning microscopy. J. Appl. Phys. 59, 3318–3327.

Ehrhardt, A.G., Kang, H.C., Tuft, R.A., Fay, F.S., Ikebe, M., 1998. Labeling of calmodulin with a new bifunctional bodipy for improved fluorophore stability in anisotropy measurements. Biophys. J. 74, A380.

Empedocles, S.A., Neuhauser, R., Bawendi, M.G., 1999. Three-dimensional orientation measurements of symmetric single chromophores using polarization microscopy. Nature 399, 126–130.

Fass, D., Bogden, C.E., Berger, J.M., 1999. Quaternary changes in topoisomerase II may direct orthogonal movement of two DNA strands. Nat. Struct. Biol. 6, 322–326.

Forkey, J.N., Quinlan, M.E., Corrie, J.E.T., Goldman, Y.E., 1999. Single-molecule structural dynamics by fluorescence polarization microscopy. Biophys. J. 76, A20.

Funatsu, T., Harada, Y., Tokunaga, M., Saito, K., Yanagida, T., 1995. Imaging of single fluorescent molecules and individual ATP turnovers by single myosin molecules in aqueous solution. Nature 374, 555–559.

Goldman, Y.E., 1998. Wag the tail: structural dynamics of actomyosin. Cell 93, 1–4.

Griffin, B.A., Adams, S.R., Tsien, R.Y., 1998. Specific covalent labeling of recombinant protein molecules inside live cells. Science 281, 269–272.

Gutfreund, H., 1995. Kinetics for the Life Sciences. Cambridge University Press, New York.

Güttler, F., Croci, M., Renn, A., Wild, U.P., 1996. Single molecule polarization spectroscopy: pentacence in p-terphenyl. Chem. Phys. 211, 421–430.

Güttler, F., Sepiol, J., Plakhotnik, T., Mitterdorfer, A., Renn, A., Wild, U.P., 1993. Single molecule spectroscopy: fluorescence excitation spectra with polarized light. J. Lumin. 56, 29–38.

Ha, T., Enderle, Th., Chemla, D.S., Selvin, P.R., Weiss, S., 1996. Single molecule dynamics studied by polarization modulation. Phys. Rev. Lett. 77, 3979–3982.

Ha, T., Glass, J., Enderle, Th., Chemla, D.S., Weiss, S., 1998. Hindered rotational diffusion and rotational jumps of single molecules. Phys. Rev. Lett. 80, 2093–2096.

Ha, T., Laurence, T.A., Chemla, D.S., Weiss, S., 1999a. Polarization spectroscopy of single fluorescent molecules. J. Phys. Chem. B 103, 6839–6850.

Ha, T., Ting, A.Y., Liang, J., Caldwell, W.B., Deniz, A.A., Chemla, D.S., Schultz, P.G., Weiss, S., 1999b. Single-molecule fluorescence spectroscopy of enzyme conformational dynamics and cleavage mechanism. Proc. Natl. Acad. Sci. USA 96, 893–898.

Harms, G.S., Sonnleitner, M., Schütz, G.J., Gruber, H.J., Schmidt, Th., 1999. Single-molecule anisotropy imaging. Biophys. J. 77, 2864–2870.

Haugland, R.P., 1996. In: Spence, M.T.Z. (Ed.), Handbook of Fluorescent Probes and Research Chemicals, 6th Edition. Molecular Probes Inc, Eugene, OR, pp. 7–46.

Heim, R., Tsien, R.Y., 1996. Engineering green fluorescent protein for improved brightness, longer wavelengths, and fluorescence resonance energy transfer. Curr. Biol. 6, 178–182.

Hellen, E.H., Axelrod, D., 1987. Flourescence emission at dielectric and metal-film interfaces. J. Opt. Soc. Am. B. 4, 337–350.

Hirschfeld, T., 1976. Optical microscopic observation of single small molecules. Appl. Opt. 15, 2965–2966.

Hopkins, S.C., Sabido-David, C., Corrie, J.E.T., Irving, M., Goldman, Y.E., 1998. Fluorescence polarization transients from rhodamine isomers on the myosin regulatory light chain in skeletal muscle fibers. Biophys. J. 74, 3093–3110.

Houdusse, A., Kalabokis, V.N., Himmel, D., Szent-Gyorgyi, A.G., Cohen, C., 1999. Atomic structure of scallop myosin subfragment S1 complexed with MgADP: a novel conformation of the myosin head. Cell 97, 459–470.

Howard, J., Hunt, A.J., Baek, S., 1993. Assay of microtubule movement driven by single kinesin molecules. Methods Cell Biol. 39, 137–147.

Hubbell, W.L., Mchaourab, H.S., Altenbach, C., Lietzow, M.A., 1996. Watching proteins move using site-directed spin labeling. Structure 4, 779–783.

Iler, R.K., 1979. The Chemistry of Silica. Solubility, Polymerization, Colloid, and Surface Properties, and Biochemistry. Wiley, New York.

Inoué, S., Spring, K.R., 1997. Video Microscopy. The Fundamentals 2nd Edition.. Plenum Press, New York.

Jenkins, F.A., White, H.E., 1976. Fundamentals of Optics 4th Edition. McGraw-Hill, New York.

Johnson, I., 1998. Fluorescent probes for living cells. Histochem. J. 30, 123–140.

Kinosita Jr., K., Itoh, H., Ishiwata, S., Hirano, K., Nishizaka, T., Hayakawa, T., 1991. Dual-view microscopy with a single camera: real-time imaging of molecular orientations and calcium. J. Cell Biol. 115, 67–73.

Lakowicz, J.R., 1999. Principles of Fluorescence Spectroscopy, 2nd Edition. Plenum Press, New York.

Loots, E., Isacoff, E.Y., 1998. Protein rearrangements underlying slow inactivation of the Shaker K+ channel. J. Gen. Physiol. 112, 377–389.

Lu, H.P., Xun, L., Xie, X.S., 1998. Single-molecule enzymatic dynamics. Science 282, 1877–1882.

Macklin, J.J., Trautman, J.K., Harris, T.D., Brus, L.E., 1996. Imaging and time-resolved spectroscopy of single molecules at an interface. Science 272, 255–258.

Mannuzzu, L.M., Moronne, M.M., Isacoff, E.Y., 1996. Direct physical measure of conformational rearrangement underlying potassium channel gating. Science 271, 213–216.

Maxfield, F.R., 1989. Fluorescent analogs of peptides and hormones. Methods Cell Biol. 29, 13–28.

Mchaourab, H.S., Lietzow, M.A., Hideg, K., Hubbell, W.L., 1996. Motion of spin-labeled side chains in T4 lysozyme. Correlation with protein structure and dynamics. Biochemistry 35, 7692–7704.

Mendelson, R., Wilson, M.G.A., 1987. Chapter 4: Fluorescence polarization studies of myosin and muscle cross-bridges. In: Baskin, R.J., Yeh, Y. (Eds.), Optical Studies of Muscle Cross-Bridges. CRC Press, Boca Raton, FL, pp. 67–98.

Moerner, W.E., Kador, L., 1989. Optical detection and spectroscopy of single molecules in a solid. Phys. Rev. Lett. 62, 2535–2538.

Moerner, W.E., Orrit, M., 1999. Illuminating single molecules in condensed matter. Science 283, 1670–1676.

Mollaaghababa, R., Steinhoff, H-J., Hubbell, W.L., Khorana, H.G., 2000. Time-resolved site-directed spin-labeling studies of bacteriorhodopsin: loop-specific conformational changes in M. Biochemistry 39, 1120–1127.

Morikawa, K., Yanagida, M., 1981. Visualization of individual DNA molecules in solution by light microscopy: DAPI staining method. J. Biochem. 89, 693–696.

Nie, S., Zare, R.N., 1997. Optical detection of single molecules. Annu. Rev. Biophys. Biomol. Struct. 26, 567–596.

Orrit, M., Bernard, J., 1990. Single pentacene molecules detected by fluorescence excitation in a *p*-terphenyl crystal. Phys. Rev. Lett. 65, 2716–2719.

Orrit, M., Bernard, J., Personov, R.I., 1993. High-resolution spectroscopy of organic molecules in solids: from fluorescence line narrowing and hole burning to single molecule spectroscopy. J. Phys. Chem. 97, 10256–10268.

Ostap, E.M., White, H.D., Thomas, D.D., 1993. Transient detection of spin-labeled myosin subfragment 1 conformational states during ATP hydrolysis. Biochemistry 32, 6712–6720.

Pawley, J.B., 1995. Handbook of Biological Confocal Microscopy, 2nd Edition. Plenum Press, New York.

Pervushin, K., Riek, R., Wider, G., Wüthrich, K., 1997. Attenuated T_2 relaxation by mutual cancellation of dipole-dipole coupling and chemical shift anisotrophy indicates an avenue to NMR structures of very large biological macromolecules in solution. Proc. Natl. Acad. Sci. USA 94, 12366–12371.

Pierce, D.W., Hom-Booher, N., Vale, R.D., 1997. Imaging individual green fluorescent proteins. Nature 388, 338.

Quinlan, M.E., Forkey, J.N., Corrie, J.E.T., Goldman, Y.E., 1999. Tilting of the light chain region in single myosin molecules using total internal reflection fluorescence polarization microscopy. Biophys. J. 76, A165.

Rayment, I., Holden, H.M., Whittaker, M., Yohn, C.B., Lorenz, M., Holmes, K.C., Milligan, R.A., 1993a. Structure of the actin-myosin complex and its implications for muscle contraction. Science 261, 58–65.

Rayment, I., Rypniewski, W.R., Schmidt-Bäse, K., Smith, R., Tomchick, D.R., Benning, M.M., Winkelmann, D.A., Wesenberg, G., Holden, H.M., 1993b. Three-dimensional structure of myosin subfragment-1: a molecular motor. Science 261, 50–58.

Rodnina, M.V., Savelsbergh, A., Wintermeyer, W., 1999. Dynamics of translation on the ribosome: molecular mechanics of translocation. FEMS Microbiol. Rev. 23, 317–333.

Ruiter, A.G.T., Veerman, J.A., Garcia-Parajo, M.F., van Hulst, N.F., 1997. Single molecule rotational and translational diffusion observed by near-field scanning optical microscopy. J. Phys. Chem. 101, 7318–7323.

Sabido-David, C., Hopkins, S.C., Saraswat, L.D., Lowey, S., Goldman, Y.E., Irving, M., 1998. Orientation changes of fluorescent probes at five sites on the myosin regulatory light chain during contraction of single skeletal muscle fibres. J. Mol. Biol. 279, 387–402.

Saito, K., Tokunaga, M., Iwane, A., Yanagida, T., 1997. Polarization measurements of single fluorophores attached to motor protein in aqueous solution. Biophys. J. 72, A179.

Sase, I., Miyata, H., Corrie, J.E.T., Craik, J.S., Kinosita Jr., K., 1995. Real time imaging of single fluorophores on moving actin with an epifluorescence microscope. Biophys. J. 69, 323–328.

Sase, I., Miyata, H., Ishiwata, S., Kinosita Jr., K., 1997. Axial rotation of sliding actin filaments revealed by single-fluorophore imaging. Proc. Natl. Acad. Sci. USA 94, 5646–5650.

Schlichting, I., Almo, S.C., Rapp, G., Wilson, K., Petratos, K., Lentfer, A., Wittinghofer, A., Kabsch, W., Pai, E.F., Petsko, G.A., Goody, R.S., 1990. Time-resolved X-ray crystallographic study of the conformational change in Ha-Ras p21 protein on GTP hydrolysis. Nature 345, 309–315.

Schmidt, Th., Schütz, G.J., Baumgartner, W., Gruber, H.J., Schindler, H., 1995. Characterization of photophysics and mobility of single molecules in fluid lipid membrane. J. Phys. Chem. 99, 17662–17668.

Scholey, J.M., 1993. Methods in Cell Biology Volume 39 Motility Assays for Motor Proteins. Academic Press, Inc., New York.

Schütz, G.J., Schindler, H., Schmidt, Th., 1997. Imaging single-molecule dichroism. Opt. Lett. 22, 651–653.

Shera, E.B., Seitzinger, N.K., Davis, L.M., Keller, R.A., Soper, S.A., 1990. Detection of single fluorescent molecules. Chem. Phys. Lett. 174, 553–557.

Soper, S.A., Shera, E.B., Martin, J.C., Jett, J.H., Hahn, J.H., Nutter, H.L., Keller, R.A., 1991. Single-molecule detection of rhodamine 6G in ethanolic solutions using continuous wave laser excitation. Anal. Chem. 63, 432–437.

Swaminathan, R., Hoang, C.P., Verkman, A.S., 1997. Photobleaching recovery and anisotropy decay of green fluorescent protein GFP-S65T in solution and cells: cytoplasmic viscosity probed by green fluorescent protein translational and rotational diffusion. Biophys. J. 72, 1900–1907.

Sytnik, A., Vladimirov, S., Jia, Y., Li, L., Cooperman, B.S., Hochstrasser, R.M., 1999. Peptidyl transferase center activity observed in single ribosomes. J. Mol. Biol. 285, 49–54.

Thompson, N.L., McConnell, H.M., Burghardt, T.P., 1984. Order in supported phospholipid monolayers detected by the dichroism of fluorescence excited with polarized evanescent illumination. Biophys. J. 46, 739–747.

Trautman, J.K., Macklin, J.J., 1996. Time-resolved spectroscopy of single molecules using near-field and far-field optics. Chem. Phys. 205, 221–229.

Trautman, J.K., Macklin, J.J., Brus, L.E., Betzig, E., 1994. Near-field spectroscopy of single molecules at room temperature. Nature 369, 40–42.

Tsien, R.Y., 1998. The green fluorescent protein. Annu. Rev. Biochem. 67, 509–544.

Unger, M., Kartalov, E., Chiu, C-S., Lester, H.A., Quake, S.R., 1999. Single-molecule fluorescence observed with mercury lamp illumination. BioTechniques 27, 1008–1014.

Vallee, R.B., 1998. Methods in Enzymology: Volume 298 Molecular Motors and the Cytoskeleton Part B. Academic Press, San Diego.

van der Heide, U.A., Orbons, B., Gerritsen, H.C., Levine, Y.K., 1992. The orientation of transition moments of dye molecules used in fluorescence studies of muscle systems. Eur. Biophys. J. 21, 263–272.

VanderMeulen, D.L., Nealon, D.G., Gratton, E., Jameson, D.M., 1990. Excitation wavelength dependent fluorescence anisotropy of eosin-myosin adducts. Biophys. Chem. 36, 177–184.

Waggoner, A., 1995. Covalent labeling of proteins and nucleic acids with fluorophores. Methods Enzymol. 246, 362–373.

Walker, J.E., 1994. The regulation of catalysis in ATP synthase. Curr. Opin. Struct. Biol. 4, 912–918.

Wand, A.J., Ehrhardt, M.R., Flynn, P.F., 1998. High-resolution NMR of encapsulated proteins dissolved in low-viscosity fluids. Proc. Natl. Acad. Sci. USA 95, 15299–15302.

Wang, Y-L., 1989. Fluorescent analog cytochemistry: tracing functional protein components in living cells. Methods Cell Biol. 29, 1–12.

Warshaw, D.M., Hayes, E., Gaffney, D., Lauzon, A-M., Wu, J., Kennedy, G., Trybus, K., Lowey, S., Berger, C., 1998. Myosin conformational states determined by single fluorophore polarization. Proc. Natl. Acad. Sci. USA 95, 8034–8039.

Weiss, S., 1999. Fluorescence spectroscopy of single biomolecules. Science 283, 1676–1683.

Xie, X.S., Dunn, R.C., 1994. Probing single molecule dynamics. Science 265, 361–364.

Xie, X.S., Trautman, J.K., 1998. Optical studies of single molecules at room temperature. Annu. Rev. Phys. Chem. 49, 441–480.

Yang, N., George Jr., A.L., Horn, R., 1996. Molecular basis of charge movement in voltage-gated sodium channels. Neuron 16, 113–122.

Yang, T.-T., Sinai, P., Green, G., Kitts, P.A., Chen, Y.-T., Lybarger, L., Chervenak, R., Patterson, G.H., Piston, D.W., Kain, S.R., 1998. Improved fluorescence and dual color detection with enhanced blue and green variants of the green fluorescent protein. J. Biol. Chem. 273, 8212–8216.

Yariv, A., 1975. Quantum Electronics, 2nd Edition. Wiley, New York.

Yasuda, R., Noji, H., Kinosita Jr., K., Yoshida, M., 1998. F_1-ATPase is a highly efficient molecular motor that rotates with discrete 120° steps. Cell 93, 1117–1124.